HHS Public Access

Author manuscript

Neuroimage. Author manuscript; available in PMC 2018 July 01.

Published in final edited form as:

Neuroimage. 2017 July 01; 154: 43–58. doi:10.1016/j.neuroimage.2016.09.007.

Noise concerns and post-processing procedures in cerebral blood flow (CBF) and cerebral blood volume (CBV) functional magnetic resonance imaging

Manus J. Donahue[1,2,3,*], **Meher R. Juttukonda**[1], and **Jennifer M. Watchmaker**[1]

[1]Radiology and Radiological Sciences, Vanderbilt University School of Medicine, Nashville, TN, USA

[2]Neurology, Vanderbilt University School of Medicine, Nashville, TN, USA

[3]Psychiatry, Vanderbilt University School of Medicine, Nashville, TN, USA

Abstract

Functional neuroimaging with blood oxygenation level-dependent (BOLD) contrast has emerged as the most popular method for evaluating qualitative changes in brain function in humans. At typical human field strengths (1.5–3.0 Tesla), BOLD contrast provides a measure of changes in transverse water relaxation rates in and around capillary and venous blood, and as such provides only a surrogate marker of brain function that depends on dynamic changes in hemodynamics (e.g., cerebral blood flow and volume) and metabolism (e.g., oxygen extraction fraction and the cerebral metabolic rate of oxygen consumption). Alternative functional neuroimaging methods that are specifically sensitive to these constituents of the BOLD signal are being developed and applied in a growing number of clinical and neuroscience applications of quantitative cerebral physiology. These methods require additional considerations for interpreting and quantifying their contrast responsibly. Here, an overview of two popular methods, arterial spin labeling and vascular space occupancy, is presented specifically in the context of functional neuroimaging. Appropriate post-processing and experimental acquisition strategies are summarized with the motivation of reducing sensitivity to noise and unintended signal sources and improving quantitative accuracy of cerebral hemodynamics.

Introduction

Magnetic resonance imaging (MRI) has been widely applied over the past three decades to obtain a more thorough understanding of the central nervous system. In addition to being an excellent tool for structural tissue characterization, functional MRI (fMRI) can be used to measure regional and global cerebral hemodynamics and to make inferences regarding

[*]**Corresponding author**. Manus J. Donahue, Vanderbilt University Institute of Imaging Science, Department of Radiology and Radiological Sciences, 1161 21st Ave South, Nashville, TN, USA, Tel: +1 615.322.8350, Fax: +1 615.322.0734, mj.donahue@vanderbilt.edu.

neuronal activity (Buxton et al., 2004; Donahue et al., 2009a; Kim et al., 2004; Ogawa et al., 1990; van Zijl et al., 1998). fMRI, which most commonly exploits blood oxygenation level-dependent (BOLD) contrast (Ogawa et al., 1990), does not require exogenous contrast agents and therefore is an invaluable tool for obtaining repeated functional measurements, assessing longitudinal changes in brain function, and for probing pathophysiological mechanisms in clinical scenarios where contrast agents may be contraindicated. As a result, BOLD fMRI has emerged as the most popular method for assessing brain function with a wide variety of clinical, pharmacological and neuroscience applications to date (Demirci et al., 2008; Fox and Raichle, 2007; Hennig et al., 2003; Jezzard and Buxton, 2006; Li et al., 2007; Martuzzi et al., 2010).

However, the BOLD fMRI signal is only an indirect marker of neuronal activity, arising from complex neurochemical, metabolic, and hemodynamic modulations that occur concurrently to both ongoing and stimulus-evoked neuronal activity (Figure 1). Specifically, in stimulus-evoked experiments, BOLD contrast arises owing to a greater increase in cerebral blood flow (CBF; ml blood / 100g tissue / min) relative to the cerebral metabolic rate of oxygen ($CMRO_2$; ml oxygen / 100g tissue / min), leading to an increase in diamagnetic oxyhemoglobin relative to paramagnetic deoxyhemoglobin in capillaries and veins (Buxton et al., 2004; Ogawa et al., 1990; van Zijl et al., 1998). In addition, low frequency (<0.1 Hz) spontaneous BOLD fluctuations, which persist in the absence of administered stimuli, are temporally correlated within known functional networks (Smith et al., 2010) and with evoked brain responses (Donahue et al., 2012a), and have been reported to be altered in a range of cognitive disorders (Fox and Raichle, 2007; Rogers et al., 2010; Smith et al., 2010; Zhang and Raichle, 2010).

While much progress has been made in understanding the hemodynamic and metabolic contributions to BOLD contrast, important gaps remain in our ability to relate BOLD signal to underlying neuronal activity and neurotransmission. These gaps significantly hinder interpretability of BOLD contrast in many applications as substantial variability in BOLD responses exists between even healthy individuals (Donahue et al., 2010a; Kannurpatti et al., 2011), partly accounting for why BOLD data remain largely qualitative in nature. Understanding the physiological sources of this variability is crucial to using BOLD as a tool for identifying quantitative differences in brain function between individuals and conditions and for gauging functional response to disease and treatment. Furthermore, non-MRI functional imaging approaches, such as positron emission tomography (PET), similarly seek to infer neuronal conclusions from surrogate hemodynamic and metabolic contrast; therefore, understanding the relationship between neuronal, hemodynamic and metabolic activity is of relevance beyond BOLD fMRI.

The critical barrier to characterizing BOLD signal is that contrast is fueled by a variety of sources, with few direct observables. However, alternative fMRI approaches specifically sensitive to individual hemodynamic parameters (Lu et al., 2003; Williams et al., 1992) can be applied in sequence with BOLD fMRI for more comprehensive investigations (Blicher et al., 2012; Buxton et al., 2004; Chiarelli et al., 2007; Detre et al., 1992; Donahue et al., 2009a; Gu et al., 2005; Kim et al., 2005; Lu et al., 2003, 2004b; Stefanovic and Pike, 2005; Williams et al., 1992; Wu et al., 2010). Much work has focused on validating the contrast of

these approaches with more established invasive techniques (Chen et al., 2008; Uh et al., 2010) and multi-modal imaging is becoming increasingly feasible. Furthermore, multimodal calibration procedures which incorporate independent measurements of hemodynamic reactivity (Davis et al., 1998) or metabolic state (Lu et al., 2010) have shown potential for characterizing BOLD signal variability.

This paper outlines considerations for quantifying CBF and CBV from the CBF-weighted arterial spin labeling (ASL) and CBV-weighted vascular space occupancy (VASO) time course, respectively. First, an overview of CBF and CBV regulation is provided, with a focus on neurophysiology and the range of changes and temporal responses of these parameters. Next, details regarding accurate quantification of CBF and CBV functional data are provided as well as an overview of currently-accepted quantification models and physiological parameters. The overall goal of this review is to summarize general guidelines for processing functional CBF and CBV data, which may serve as a reference for investigators seeking to complement or replace BOLD fMRI with these approaches.

Physiology of cerebral blood flow and volume regulation

Before detailing these methods and the relevant considerations, it is first useful to review the physiological meaning of the parameters interest.

Oxygenated blood is delivered to the brain tissue primarily through the internal carotid arteries (ICA) and vertebral arteries, which supply blood to the majority of anterior and posterior brain parenchyma, respectively. In the absence of a moderate stenosis (e.g., luminal narrowing of 50% or more), such blood is delivered at a high peak systolic velocity of up to 125 cm/s in the ICAs and 50 cm/s in the vertebral arteries (Seidel et al., 1999). As blood enters the cerebral microvasculature, the blood velocity drops to approximately 10 cm/s for arteries on the order of 1 mm in diameter and further to < 1 cm/s for small arterioles on the order of <100 μm in diameter (for a review see: (Piechnik et al., 2008)). Importantly, the smooth muscle that lines arterioles permits relaxation and constriction of the arterioles to meet the local energy demands of the surrounding tissue. These arterioles feed the capillary bed (diameter of approximately 5–10 μm) where restricted exchange between the blood and tissue compartments is permitted; here, nutrients such as oxygen and glucose enter the tissue and waste products such as CO_2 and other metabolic byproducts are taken up by the capillaries and exit the brain through the venous system. While not a direct measure of neuronal activity, changes in blood delivery, mediated largely by vasodilatory intermediaries occurring as byproducts of elevated energy metabolism and neurotransmission, provide a surrogate marker of changes in metabolic and neuronal activity under most conditions (Guyton, 1977; Powers et al., 1985).

CBF describes the rate at which blood is delivered to tissue and is frequently measured in units of ml blood / 100g of tissue / minute. Note that this is not a measure of blood flow velocity (cm/s), which is frequently measured using quantitative phase contrast MR angiography or ultrasound-based methodologies, but rather a tissue-level measure of the rate of blood delivery to the tissue. Healthy adult gray matter CBF values are generally reported in the range of 40–60 ml/100g/min, and white matter CBF values are reported in the range

of 10–30 ml/100g/min or approximately 2–3 fold less than gray matter CBF values (Grubb et al., 1974). Functional hyperemia in response to strong neuronal stimuli such as finger tapping or visual flashing checkerboard is commonly reported in the range of 5–100% (increase over baseline) for healthy parenchyma and is predominately localized to gray matter parenchyma (Donahue et al., 2009a; Hua et al., 2011a; Huber et al., 2015b; Lu et al., 2004b); for typical vascular stimuli such as mild hypercapnia (increases in arterial carbon dioxide tension, $PaCO_2$, of 10 mmHg or less), the CBF increases by approximately 1–2 ml/100g/min per 1 mmHg increase in $PaCO_2$ (Grubb et al., 1974), however this response can vary between subjects and with basal hemodynamic state.

CBV describes the volume of blood within a brain region, and is most commonly reported in units of ml blood / ml parenchyma (ml/ml). Typical gray and white matter CBV values are in the range of 0.04–0.06 ml/ml and 0.01–0.03 ml/ml (Donahue et al., 2010b; Grubb et al., 1978; Herold et al., 1986), respectively. The CBV within a parenchymal voxel is roughly comprised of 30% arterial (e.g., pre-capillary; oxygenation levels of 0.95–1.00) and 70% venous (e.g., post-capillary; oxygenation levels of 0.55–0.65) (van Zijl et al., 1998). The CBV response to hyperemia is largely coupled to the CBF response in healthy parenchyma, and most commonly described by a power law relationship of $CBV \sim CBF^{\alpha}$ where α is the Grubb-coefficient, reported in the range of 0.38–0.50 (Eichling et al., 1975; van Zijl et al., 1998).

Functional neuroimaging based on quantitative hemodynamic or metabolic contrasts, rather than qualitative BOLD contrast, requires a fundamentally different perspective for how the data are analyzed and interpreted. Specifically, while the goal of the majority of BOLD fMRI analysis procedures is to maximize the statistical power of any detectable response, frequently by titivating the data through various post-processing steps such as spatial or temporal filtering, noise pre-whitening, and co-registration or resampling, the goal of quantitative hemodynamic analysis is to accurately *quantify* the signal changes, which provides a measure of quantitative CBF or CBV reactivity. As such, methods that may increase the statistical significance of an evoked response, but fundamentally change the underlying data, may be undesirable.

Quantitative functional neuroimaging measures of cerebral blood flow (CBF) using arterial spin labeling (ASL)

ASL fMRI has emerged as a popular alternative to BOLD fMRI owing to its ability to quantify a single physiological parameter in absolute units, namely cerebral blood flow (CBF; rate of blood water delivered to tissue). As described in the previous section, CBF changes are closely related to energy demand and therefore CBF provides a surrogate marker of neuronal activity in most situations. CBF is also impacted by changes in cerebral perfusion pressure secondary to arterial steno-occlusion, and, therefore, ASL has been widely applied in the setting of cerebrovascular disease (Detre and Wang, 2002; Donahue et al., 2012b) to identify abnormal neurovascular coupling mechanisms (Blicher et al., 2012; Donahue et al., 2010a), flow territory asymmetry (Donahue et al., 2014c; Faraco et al., 2015a; Hendrikse et al., 2005; Okell et al., 2013), and lateralizing steno-occlusive disease

(Donahue et al., 2014a; Faraco et al., 2015a; Zaharchuk et al., 2011). In addition, ASL has good correspondence with more standard, invasive clinical measures of disease severity such as catheter angiography and gadolinium perfusion MRI (Donahue et al., 2012b; Warmuth et al., 2003).

In ASL, arterial blood water is magnetically labeled using one or multiple radiofrequency (RF) pulses (Williams et al., 1992), after which a delay time is allowed where the blood water enters a region of interest and exchanges with tissue water. Due to the RF label, the blood water will attenuate the tissue water signal after exchange. CBF-weighted contrast can then be obtained by comparing this labeled image with an image where blood water is not labeled. In functional experiments, ASL generally has higher timecourse stability than BOLD fMRI for long duration block designs (Aguirre et al., 2002), and owing to its quantitative and noninvasive contrast mechanism is ideally suited for evaluating longitudinal changes.

Disadvantages of ASL fMRI primarily pertain to the much lower signal-to-noise ratio (SNR) relative to BOLD as well as to the multiple ASL variants available and variations in quantified CBF values obtained from these variants (Detre et al., 2009). Additionally, the short delay time required (1–2.5s) limits the ability of ASL to detect blood with arrival times of greater than approximately 2.5s, hindering the utility of this metric in subjects where blood arrival times may be delayed due to pathology. However, owing to the large CBF response for most functional stimuli (5–20 ml/100g/min for strong vascular or neuronal stimuli), ASL contrast-to-noise ratio (CNR) is very similar to BOLD CNR, as BOLD signal changes are on the order of a few percent only. In addition, the International Society for Magnetic Resonance in Medicine (ISMRM) Perfusion Study Group very recently released a white paper (Alsop et al., 2014) outlining optimal imaging parameters for the two most practical ASL variants: Pulsed ASL (PASL) with QUIPSSII (Wong et al., 1998) and pseudo-continuous ASL (pCASL) (Dai et al., 2008).

Here, confounds to the ASL signal and corresponding CBF quantification are summarized, and their graphical impact on a simulated typical CBF response is shown in Figure 2. The procedure that is recommended for removing these confounds in ASL data is summarized in the following steps below and outlined in more detail in the following sections:

- *Experimental.* Acquire ASL data using long (>1600 ms) inversion time (TI) pulsed ASL (PASL) or post-labeling delay (PLD) pseudo-continuous (pCASL). The purpose of these waiting times is to allow for labeled cervical blood water to have sufficient time to exchange with the tissue water in the capillary bed. In subjects with high flow velocities (e.g., sickle cell anemia), this time may be reduced to improve temporal resolution, whereas in individuals with longer blood arrival times (e.g., arterial steno-occlusion or chronic ischemia), this time may require lengthening. As the magnetic label decays with the T_1 of arterial blood water (approximately 1.7s at 3.0T), post-labeling waiting times longer than 2–2.5s at typical field strengths (e.g., 3.0T) are generally not recommended owing to low SNR.

- *Experimental.* Acquire a separate equilibrium magnetization (M_0) image, which has identical spatial resolution and readout as the ASL acquisition but long TR of 15–20s to ensure that the tissue component with the longest T_1 (generally CSF; 3.0T T_1~4.3s) has recovered to equilibrium. Ensure that scanner gain, shimming, and any scaling has not been reset between the ASL and M_0 acquisition.
- *Post-processing.* Correct magnitude ASL data for motion using for example standard affine routines, commonly used in BOLD fMRI. This step must be performed prior to pair-wise subtraction or further processing.
- *Post-processing.* Perform pair-wise subtraction of the control and label images. In the case of functional acquisitions where blood oxygenation level may vary between control and label acquisitions (e.g., near the onset or cessation of stimulus), such data should either be removed or corrected for blood oxygenation level using surround-subtraction procedures described below.
- *Post-processing.* Perform quality control of each subtracted control/label pair, to ensure that residual motion that was too substantial to be accounted for in the above motion correction routines does not bias the corresponding time course. Such motion artifacts may be present at a higher rate when a functional stimulus (e.g., joystick movement, hypercapnic gas challenge, pain stimulus, etc.) begins or ends.
- *Post-processing.* The time course of subtracted control/label pairs, i.e., the difference magnetization, can be converted to CBF in absolute units of ml/100g/min by applying the solution to either the simplified one-compartment (Alsop et al., 2014) or two-compartment (Wang et al., 2002) flow-modified Bloch equation and including the M_0. Assumptions regarding blood arrival time may need to be considered and are outlined below, however these issues are generally not incorporated into recently recommended simplified quantification models.
- *Post-processing.* If multiple identical blocks of the functional stimuli are repeated, block-average the CBF time course to improve SNR if desired.
- *Post-processing.* Evaluate the mean time course (e.g., mean of each individual block stimulus) and ensure that CBF changes are within the range of expected physiological changes (Table 1). Importantly, if the CBF changes are too large, this is an indicator that there was an error in acquisition or post-processing, and the above steps should be re-evaluated.
- *Post-processing.* If comparing CBF changes with BOLD or other functional changes, it is important to analyze exactly the same voxels, as CBF, CBV, and venous architecture may differ substantially between voxels. Common approaches are to analyze only the subset of voxels meeting a defined activation criterion in all functional acquisitions or rather to use an anatomical region-of-interest. The former functional localizer approach will often bias the analysis to voxels with larger venous contributions in BOLD data, whereas the latter anatomical approach may underestimate hemodynamic responses if voxels that

are not hemodynamically active are included. It is often useful to incorporate both analysis approaches (Faraco et al., 2015b).

Below we include additional information on the post-processing steps and details of this analysis, as appropriate ASL acquisition has recently been reviewed already (Alsop et al., 2014).

Motion correction

Like with BOLD fMRI, motion is a concern and should be addressed in ASL experiments. In many ways, ASL is even more sensitive to motion than BOLD as motion between control/label pairs can result in very high subtraction errors and physiologically unreasonable CBF values. Motion artifacts are discernable in the subtracted image and manifest frequently as a bright ring around perimeter of the brain, which may encircle the entire brain or only a fraction, depending on the direction of the motion. This issue should be considered with more care in functional ASL data, as the signal at a given time point may be of interest. This is in contrast to baseline ASL acquisitions that simply average over a long, repeated acquisition of control/label pairs, in which mild motion artifacts may not be overly detrimental to the final mean CBF map.

As unsubtracted ASL images are most commonly intermediate echo time (TE ~ 10–25 ms at typical spatial resolutions) T_2*-weighted images, motion correction algorithms that have been optimized for BOLD analysis (TE ~ 30 – 45 ms at 1.5T–3.0T) can also be applied to the pre-subtracted ASL images reliably. Note that ASL images generally benefit from shorter TEs where SNR is higher and sensitivity to susceptibility and BOLD effects is lower. These algorithms generally focus on principles of affine, intramodal brain registration (Jenkinson et al., 2002).

More recently alternative strategies have also been developed that focus on interrogating the quality of subtracted control/label pairs and weighting corresponding block-averaged ASL data based on a noise or motion estimate (Tanenbaum et al., 2015). Additional approaches are being developed that use navigator images to prospectively correct for motion (Frost et al., 2015; Zun et al., 2014); such navigators generally acquire only a fraction of k-space and can be incorporated by adding little (<300 ms) or no additional scan time, thereby having only a small influence on temporal resolution of the ASL acquisition. These prospective motion-correction routines are not commonly incorporated into ASL acquisitions due to expertise required in programming, however it is reasonable that such acquisition-based corrections will become more standardized in the next several years.

Motion in the subtracted ASL images frequently manifest as a bright, contiguous artifact surrounding the brain tissue. The images should be inspected for these artifacts, and if the above correction procedures are insufficient to remove such artifacts, these specific control/label pairs should be discarded as these data could bias true CBF responses.

The result of this first stage of post-processing should be a time-course of motion-corrected, short-TE gradient echo images, with interleaved perfusion weighting.

Subtraction strategies

To convert the motion-corrected magnitude ASL data to CBF-weighted maps, it is necessary to subtract the label image, where the lower blood water magnetization attenuates the tissue water signal after exchange, from the control image, in which blood and tissue water magnetization are near equilibrium. To achieve this, control and label images, which are acquired sequentially, can be simply pair-wise subtracted in non-functional ASL scans. In functional scans the situation is slightly more complex. Specifically, while the TE in ASL acquisitions is relatively short (generally 10–25 ms in most single-shot gradient echo 2D EPI acquisitions), this is a sufficient time to allow for BOLD effects to occur; e.g., increases in capillary, venous, and surrounding tissue water T_2* secondary to fractional reductions in paramagnetic deoxy-hemoglobin in capillary and venous blood water. Differences in blood oxygenation level between sequential control and label acquisitions, which are separated in time by 4–8s, may lead to artifacts in the resulting difference image, most noticeably near the transition between stimulus or baseline conditions.

These effects have been investigated in detail and appropriate post-processing procedures have been proposed, including surround subtraction approaches (Lu et al., 2006; Wong et al., 1997). In these approaches, consecutive control images are either averaged or interpolated to the time of the label image that is acquired in-between, with the intent of maintaining a similar blood oxygenation level of the resulting combined control image and the label image. This approach has been shown to reduce fluctuations in the ASL time course, especially near the onset and cessation of stimulus. An example of this effect is shown schematically in Figure 2.

The result of these first two-steps should be a motion-corrected and blood oxygenation-corrected time course of CBF-weighted images.

ASL quantitation

One of the major advantages of ASL is that the data, if acquired and processed properly, provides a quantitative physiological value (i.e., CBF in ml blood / 100g tissue / min) rather than a more arbitrary T_2(*)-weighted signal intensity or z-statistic as is the case in BOLD fMRI. Conversion of the acquired difference magnetization from the above two steps to quantitative units of CBF requires application of the flow-modified Bloch equation, which has been presented in detail in the literature for both continuous, pulsed, and pseudo-continuous ASL variants (Alsop et al., 2014; Wang et al., 2002; Zhou et al., 2001). In this approach, the z-component of the Bloch equation is modified to include a flow term, as well as the arterial and venous longitudinal magnetization in the case of a single compartment model, or an additional tissue component in the case of a two-compartment model. A recent white paper by the ISMRM perfusion study group suggested that in most applications a simplified single-compartment kinetic model is appropriate (Alsop et al., 2014), which allows for the CBF to be solved for explicitly and eliminates the need for detailed estimates of blood arrival time to be made which in principle can vary between subjects and have a limited effect on CBF quantification over a typical range of recommended acquisition parameters (e.g., long post-labeling delay times or inversion times). This simplified model is

not accurate however if short waiting times after labeling are used, or blood water is substantially delayed in arriving at the tissue, as the underlying assumption is that the labeled blood water has had sufficient time to exchange with tissue water.

These equations can be written separately for pCASL and PASL as,

$$CBF_{pCASL}=\frac{\Delta M}{M_0}\cdot\frac{\lambda\cdot e^{PLD/T_{1,b}}}{2\cdot\alpha\cdot T_{1,b}\cdot\left(1-e^{-\tau/T_{1,b}}\right)}\cdot 6000, \quad [1]$$

and

$$CBF_{PASL}=\frac{\Delta M}{M_0}\cdot\frac{\lambda\cdot e^{TI/T_{1,b}}}{2\cdot\alpha\cdot TI_1\cdot}\cdot 6000. \quad [2]$$

Here, $\Delta M/M_0$ is the difference magnetization normalized by the separately acquired M_0 map. If a separate M_0 image is not available, it is possible to estimate the M_0 from the control image as the TR in such scans is long and gray and white matter magnetization are near equilibrium. For this purpose, the control image can be divided by the term [1-exp(−TR/$T_{1,t}$)], where TR is the repetition time and $T_{1,t}$ is the T_1 of the tissue component (Table 1). This procedure simply converts the steady-state magnetization to equilibrium magnetization by accounting for the effect of the excitation pulse. PLD is the post-labeling delay in pCASL experiments, whereas TI is the inversion time in PASL experiments. In the case of QIUPSS-II PASL, TI_1 describes the time of the slab-selective saturation pulse that is applied to control the blood water bolus duration. $T_{1,b}$ is the T_1 of blood water, α is the labeling efficiency, and τis the pCASL labeling duration. 6000 is a factor that converts from ml/g/s to more conventional units of ml/100g/min.

In functional experiments, it is worthwhile to consider two potentially confounding factors to these equations that are often neglected. First, the bolus arrival time (BAT; time for labeled blood water to exchange with tissue water) and the velocity of blood in cervical vessels may vary between baseline and stimulus conditions. The above, simplified equations do not explicitly incorporate the BAT and assume that all blood water has had sufficient time to exchange with tissue water. However, if the PLD or TI is not sufficiently long to ensure this criterion, the quantified CBF will be inaccurate. Furthermore, if functional stimuli lengthen the BAT (e.g., such as hyperoxia or pharmacological stimuli), longer waiting times may need to be incorporated.

Second, pCASL is especially sensitive to blood water velocity at the location of the labeling plane, which generally occurs approximately 90 mm inferior to the corpus callosum near the confluence of the vertebral and basilar arteries. Labeling efficiencies of approximately 85%

are frequently assumed, however this value is most appropriate for blood water flowing at healthy velocities (see *Physiology of cerebral blood flow and volume regulation*), and may reduce if the flow velocity is elevated. This effect has been quantified for elevated flow velocities secondary to anemia and reduced oxygen carrying capacity (Figure 3), and in neuronal (Gonzalez-At et al., 2000) and vascular (Donahue et al., 2014b) functional experiments, it has been shown that blood arrival times, and likely cervical velocities, will adjust slightly as well (Figure 4). In fact, for strong neuronal stimulation it has been shown that the reduction in BAT is nearly as large as the increase in CBF (Gonzalez-At et al., 2000). Post-processing strategies have been proposed for correcting for the labeling efficiency on a subject-specific basis. One strategy is to quantify the whole-brain CBF from a quantitative velocity map of blood in the major feeding arteries (left and right ICAs and vertebral arteries), integrate the velocity over the cross sectional area of the vessel to obtain a map of total blood flow (ml/s), and normalize this value by the intracranial tissue volume (Aslan et al., 2010). These data can be acquired relatively quickly in 30–120s (Liu et al., 2014). In scenarios where blood velocities or BAT are anticipated to change substantially between a baseline and activated condition, it may be useful to incorporate such procedures into pCASL quantification models.

The result of the above steps should be quantitative CBF maps that span the duration of the functional experiment. The temporal resolution of twice the scan TR results when conventional pair-wise subtraction is used, however the temporal resolution can be restored to one TR when surround subtraction is used.

Regional quantitation of ASL data

A final concern is related to the most responsible way to present functional ASL data. In BOLD fMRI experiments, it is typical to show primarily spatial regions of activation, frequently overlaid on a highresolution structural image or atlas. While this can also be done in ASL, the process of co-registration and associated spatial smoothing will generally reduce the CBF values by 5–10%, owing primarily to smoothing of the CBF values across gray matter, white matter, and CSF. While this can still be useful for evaluating group-level differences visually, or performing spatial statistical tests, these analyses should be applied with caution when the populations may have differing levels of atrophy that could in turn influence the final quantified CBF maps.

It is also useful to show the associated CBF time course (Figure 5 **and** 6) for two reasons. First, it ensures that the measured CBF responses are within a physiologically meaningful range, reinforcing the credibility of the data and the specific acquisition and post-processing pipeline. Second, temporal features of the CBF response, such as onset or reduction times, or potential post-stimulus compensatory effects can be evaluated, which may provide additional information beyond simple magnitude responses (Ances et al., 2009; Donahue et al., 2009c; Lu et al., 2004b).

Frequently time courses are compared between functional imaging modalities, such as BOLD and ASL, and voxel selection is required. This can be achieved by either using statistical thresholds for activation (e.g., from a t-test, cross-correlation test, or similar), from

commonly-available mathematical or fMRI processing toolboxes, or alternatively using an anatomical region-of-interest (e.g., all occipital gray matter). If statistical methods are used, it is important to adjust the pipeline from a typical BOLD analysis, which may involve spatial smoothing or noise pre-whitening, both of which are intended to maximize statistical efficiency but may alter the underlying quantitative CBF values. An additional concern in statistical testing is that the voxels selected will be inherently biased by composition. For instance, BOLD voxels with the highest t-statistics will almost always also contain larger venous blood volume fractions, and spatial regions of high venous blood oxygenation changes may not always co-localize well with regions of high CBF (which is more closely localized to capillary vasculature). Therefore, alternative anatomical regions-of-interest may be used. With anatomical regions-of-interest, there is less bias for the vascular compartment in principle, but it is possible that regions of limited or no activation may be included. Both regional analyses are useful to consider depending on the application and it has been shown that quantitative oxygenation levels and relaxation times can vary considerably depending on the analysis procedure that is selected (Faraco et al., 2015b).

Experimental considerations for maximizing functional ASL sensitivity

CBF functional imaging using ASL most commonly incorporates long block stimuli, rather than eventrelated stimuli, largely due to the low SNR of a single control/label difference imaging and the necessity to average multiple images to obtain sufficient SNR. Keeping in mind that a typical ASL difference image requires on average 4–8s to obtain (due to the long waiting times, associated TRs, and requirement for a control and label image; i.e., two TRs), such functional block periods are typically on the order of 30s or more depending on the SNR of any given image.

SNR can be increased considerably through the use of background suppression. In background suppression, multiple inversion pulses are applied between the labeling period and readout excitation pulse, and are appropriately spaced in time so as to maintain the longitudinal component of the tissue magnetization (two pulses for gray and white matter) near zero while not influencing substantially the state of the inflowing blood water magnetization (Mani et al., 1997; Ye et al., 2000). This maintains the CBF weighting but reduces the static tissue signal drastically and results in the subtraction of two small images, instead of two large images, to obtain the CBF weighting. Background suppression has been investigated in detail and has been shown to reduce the temporal instability of ASL images by 50% (Mani et al., 1997; Ye et al., 2000), which can be exploited to either reduce the overall number of averages required in typical ASL acquisitions or improve the interpretability of any one image in a function run. This improvement may allow for temporal characteristics of the CBF response, such as CBF onset time and any possible reduction below baseline or changes in response time after stimulus cessation, to be interrogated in more detail.

There are two general considerations when applying background suppression. First, in pCASL labeling schemes, background suppression pulses reduce the labeling efficiency from approximately 85% to 80% for typical cervical flow velocities. However, this small reduction in SNR is more than compensated for with the large increase in temporal stability.

Second, the background suppression pulses are intended to null the tissue magnetization at the time of the excitation pulse. For some 3D readouts, such as 3D GRASE (Gunther et al., 2005), there is a single excitation pulse followed by a subsecond whole-brain readout, and as such the tissue suppression is identical for all slices. For 2D EPI readouts, where the slice-specific excitation pulses are separated in time (by generally 20–40 ms for typical spatial resolutions and parallel imaging factors), the tissue suppression, and correspondingly the SNR, will vary by slice location with the slices acquired first having the highest SNR and the slices acquired last having the lowest SNR. For this reason background suppression is generally recommended for 3D readouts, but additional considerations regarding the above confounds must be taken into account when applying this in 2D EPI readouts. Strategies to address this confound could be related to altering the order of the slice acquisition across measurements or adjusting the tissue null point to correspond more closely with the middle slice rather than with the first slice; however, these alternative strategies have not been investigated in great detail.

The above experimental considerations, namely incorporation of background suppression pulses and/or higher SNR 3D readouts, are useful considerations when planning functional ASL experiments, as both sequence adjustments will improve the SNR of a single control/label pair, thereby improving the interpretability of CBF time course dynamics.

Quantitative functional neuroimaging of cerebral blood volume (CBV) using vascular space occupancy (VASO) MRI

While CBV is frequently assumed to be closely coupled to CBF through the Grubb relationship, a range of values for such coupling indices have been reported, and therefore independent measures of CBV are of interest in quantitative functional imaging experiments. Additionally, a range of autoregulatory arteriolar increases in CBV are possible in many pathological conditions, especially arterial steno-occlusive disease where microvascular CBV may increase to maintain perfusion in the presence of proximal arterial steno-occlusion and reductions in cerebral perfusion pressure. As such, the extent of CBF and CBV uncoupling may provide a valuable indicator of tissue compensation adequacy and even stroke risk (Derdeyn et al., 2002).

VASO fMRI has been proposed as a method for obtaining CBV-weighted contrast noninvasively *in vivo* (Lu et al., 2003; Lu and van Zijl, 2012). In VASO, the blood water signal is nulled and the resulting image is derived from extravascular water only. Vasodilatory CBV changes are inferred from changes in measured extravascular signal (Figure 7), which will reduce for vasodilation and increase for vasoconstriction. Much work has focused on understanding the origins of VASO contrast, and issues regarding blood water inflow and exchange (Donahue et al., 2009b; Hua et al., 2013; Lu, 2008), nulling times (Donahue et al., 2009b), partial volume contributions (Donahue et al., 2009a; Donahue et al., 2006), and multi-slice imaging (Donahue et al., 2009a; Huber et al., 2016a; Huber et al., 2014b; Lu et al., 2004c; Poser and Norris, 2009; Scouten and Constable, 2007), are now better understood. Recently, elegant applications of VASO at the high field strength of 7.0T have shown promise for improving functional localization relative to BOLD fMRI (Hua et

al., 2013; Huber et al., 2014a; Huber et al., 2014b; Huber et al., 2016b) and for probing mechanistic differences in hemodynamic properties across cortical layers (Huber et al., 2015b). Validation studies have been performed comparing VASO contrast with more established monocrystalline iron oxide nanoparticle (MION)-CBV (Jin and Kim, 2006), PET CBV (Uh et al., 2010) and gadolinium-CBV (Donahue et al., 2010b) approaches, reinforcing the CBV-weighted sensitivity of VASO.

The popularity of VASO for fMRI has not grown beyond specialized centers and therefore it is not nearly as widely used for CBV mapping as ASL fMRI is for quantitative CBF mapping. However, owing to the relative paucity of methods for noninvasive *in vivo* quantification of CBV in humans, VASO is currently the most popular noninvasive approach for CBV mapping, and a review of VASO acquisition and development has recently been published (Lu and van Zijl, 2012). Here, an overview of the VASO contrast mechanism and relevant considerations for quantifying and interpreting the VASO signal in the context of functional MRI experiments will be presented.

VASO acquisition considerations

In VASO, the blood water nulling is achieved through principles of inversion recovery; specifically, following non-selective adiabatic inversion, an image is acquired at the time when the longitudinal component of the blood water magnetization is near zero. In this sense, it is very similar to fluid-attenuated inversion recovery (FLAIR) MRI with the key difference that the inversion time is chosen to null the blood rather than cerebrospinal fluid (CSF) signal. As tissue water T_1 is shorter than blood water T_1 (Table 1), there will be residual longitudinal magnetization of 10 – 20 % of M_0 at the time of blood water nulling. The magnitude of the tissue signal, and in turn corresponding SNR, will vary with the TR and TI choice (which can be adjusted together to keep the steady-state blood water signal nulled).

In fMRI conditions, short TR and TI groupings (e.g., TR=2000 ms and TI=711 ms) can be chosen to improve temporal resolution, however it has also been shown that such short TR scans are sensitive to inflow of fresh blood water as well as potential perfusion effects (Donahue et al., 2006). The former effect is due to the steady-state blood water nulling time being much shorter than the equilibrium blood water nulling time for short TRs, and therefore short TR being especially sensitive to any fresh blood that may flow into the slice over the course of the inversion time or in subsequent scans and which therefore may not be at steady state. Note that for cases with large volume transmit coils or with animals that may fit into the entire transmit coil, this artifact is reduced. Regarding perfusion effects, it has been shown that long TR choices can reduce the magnitude of perfusion-mediated exchange effects, and these contributions have been investigated in detail in simulation and experimental studies (Donahue et al., 2006). For the combined reasons, pure CBV contrast from VASO data is more interpretable for long TR/TI combinations (e.g., TR=5000 ms or greater); however the tradeoff is that the temporal resolution of the experiment is much poorer, and as such it is difficult to obtain multiple images during short block fMRI acquisitions or to interrogate subtle temporal features of the CBV response. To minimize artifacts related to this effect, a magnetization reset module consisting of a nonselective

saturation followed by a dephasing gradient may be added to the end of the readout to reduce the effect of inflowing fresh spins (Lu, 2008). Additionally, a motion sensitized driven equilibrium module can be placed after the inversion and prior to the readout (Hua et al., 2013). This module includes 90 degree (flip down) and −90 degree (flip back) pulses surrounding refocusing pulses, which serve to destroy the phase coherence of moving spins. When these additions are included, shorter TR values (TR=2000 ms and 3000 ms) can be used with low inflow effect; appropriate imaging choices can be made depending on the physiological or functional question of interest. Many recent VASO studies use a combination of these inflow correction procedures (Cheng et al., 2015; Hua et al., 2013; Huber et al., 2015b).

VASO quantitation considerations

Unlike ASL, VASO does not provide an absolute baseline map of CBV, but rather signal changes in response to a stimulus are interpreted as a surrogate of CBV *changes*. The changes can be interpreted as absolute CBV changes in units of voxel volume (i.e., ml blood change per ml of tissue) as has recently been described for CBV mapping using exogenous contrast agents (Kim et al., 2013) or VASO (Huber et al., 2015a), or in-line with earlier theory papers by normalizing by a baseline CBV value (CBV_0) to report a fractional change in units of ml blood / ml parenchyma. The theory of such relative VASO signal changes has been presented in the original VASO manuscript (Lu et al., 2003) and expanded to include perfusion and partial volume contributions in subsequent studies (Donahue et al., 2006); the most relevant aspects are summarized here.

For a series of consecutive adiabatic inversion pulses, the steady-state solution to the zcomponent of the Bloch equation can be written,

$$M_{z,j}=M_0(1-2e^{-TI/T_{1,j}}+e^{-TR/T_{1,j}}) \text{ for } j=\text{tissue, blood, or CSF,} \quad [3]$$

where $M_{z,j}$ is the longitudinal magnetization of tissue component *j,* M_0 is the equilibrium magnetization, TI is the inversion time (time between adiabatic inversion and excitation), $T_{1,j}$ is the longitudinal relaxation time of tissue component *j,* and TR is the repetition time.

The transverse component of the magnetization can be written simply as,

$$M_{xy,j}=e^{-TE/T_{2,j}^{(*)}} \quad j=\text{tissue, blood or CSF,} \quad [4]$$

where TE is the echo time and $T_{2,j}^{(*)}$ is the transverse relaxation time (spin echo) or effective transverse relaxation time (gradient echo), depending on which acquisition is used.

At typical spatial resolutions of 2–5 mm (x, y, and/or z dimension), cortical voxels will partial volume with tissue (gray and white matter), CSF, and blood and the total signal (S) can be written explicitly in terms of these components:

$$S = X_{\text{tissue}} \cdot S_{\text{tissue}} + X_{CSF} \cdot S_{CSF} + X_{\text{blood}} \cdot S_{\text{blood}}, \quad [5]$$

for

$$S_{\text{tissue}} = C_{\text{tissue}} \cdot M_{z,\text{tissue}} \cdot M_{xy,\text{tissue}} = (C_{\text{parenchyma}} - C_b \cdot CBV) \cdot M_{z,\text{tissue}} \cdot M_{xy,\text{tissue}}, \quad [6]$$

$$S_{CSF} = C_{CSF} \cdot M_{z,CSF} \cdot M_{xy,CSF}, \quad [7]$$

and

$$S_{\text{blood}} = 0. \quad [8]$$

While CSF is not always incorporated into VASO quantification models, the CSF fraction can be large at typical spatial resolutions of 2–5 mm, and the CSF signal in long TR VASO acquisitions will be large and may even relocate between voxels between rest and activation scenarios. The CSF signal itself can be reduced in so-called VASO-FLAIR acquisitions (Donahue et al., 2009a; Donahue et al., 2006), in which a double-inversion recovery is used to simultaneously null both blood and CSF water, albeit at the cost of SNR of the tissue (Figure 7). CSF can also be eliminated in separate scans and the data combined *post-hoc* (Scouten and Constable, 2008). Furthermore, the voxel fractions of tissue and CSF can be estimated from separately-acquired T_1-weighted scans at an identical spatial resolution, and application of freely-available T_1-segmentation routines which exploit hidden Markov random field model and an associated Expectation-Maximization algorithm and are used commonly in fMRI and tissue volume segmentation studies (Zhang et al., 2001).

The CBV is most commonly quantified in VASO fMRI studies by recording the signal change in VASO from a baseline (S_0) and stimulated (S_{on}) state,

$$\frac{\Delta S}{S_0} = \frac{\left(S_{\text{tissue,on}} + S_{CSF,\text{on}}\right) - \left(S_{\text{tissue},0} + S_{CSF,0}\right)}{\left(S_{\text{tissue},0} + S_{CSF,0}\right)}. \quad [9]$$

Note that in the equation above, the blood signal has been omitted as this term is selectively nulled in the VASO experiment. The CBV can be estimated from the above equation with knowledge of the CSF volume fraction and relaxation times. If the CSF component is omitted or selectively nulled in a VASO-FLAIR experiment, then Equation 9 simplifies to,

$$\frac{\Delta S}{S_0} = \frac{C_b \cdot \Delta CBV}{C_{\text{paraenchyma}} - C_b \cdot CBV_0}. \quad [10]$$

$C_{parenchyma}$ and C_b are constants which are known (Table 1) and are not expected to change between a baseline and stimulated state, leaving only the ΔCBV (CBV_{on}-CBV_0) and CBV_0 as unknowns. CBV_0 is generally assumed in VASO experiments to be 0.047 – 0.055 ml/ml and in turn the CBV_{on} is solved for. More recent VASO variants which include a subtraction component have been proposed, and permit estimation of the CBV_0 term as well; these variants are discussed below.

Parameters used in these models are summarized in Table 1 and are also broadly applicable to ASL quantification procedures.

Inflow vascular space occupancy (iVASO)

The traditional VASO approach, described above, is achieved by performing a non-selective adiabatic inversion, which inverts all magnetization, and an image is acquired when the blood water magnetization is near zero but the tissue water magnetization is slightly positive. However, this method has inherently low SNR as the tissue water magnetization, even in conditions of long TR and equilibrium conditions, will reach a maximum value of approximately 20% of M_0 for typical field strengths of 1.5T–3.0T.

To increase the SNR, it is possible to substitute the non-selective adiabatic inversion for a slice-selective inversion inferior to the imaging volume in a so-called inflow VASO (iVASO) sequence (Hua et al., 2011a). Following this slice-selective inversion, inverted blood water will flow into the imaging volume and an image can be acquired at the null point of the blood water. Here, the static tissue water magnetization is not influenced by the inversion pulse, and therefore the tissue water magnetization is near equilibrium (attenuated only by the steady state effects of the excitation pulse) and the SNR is considerably higher. This approach has been used in functional experiments to improve SNR of single VASO images considerably, and has even been applied to interrogate differences between arterial and total CBV dynamics (Figure 8) (Hua et al., 2011a). The limitation of iVASO is that the contrast may be very sensitive to blood arrival time, and it is important to ensure that the blood water has had sufficient time to fill the capillary bed, but not yet to exchange with tissue water (e.g., perfuse). However, iVASO experiments performed at multiple inversion times have been performed and shown to be approximately arterial CBV weighted for appropriate imaging parameters (inversion times = 700 – 1100 ms) (Hua et al., 2011a; Rane et al., 2016). It should also be noted that while the blood signal in the iVASO experiment remains nulled, as in traditional VASO, the tissue signal will follow a saturation recovery rather than an inversion recovery, which should be taken into account during quantification. The details of this quantification procedure, including assumptions regarding blood arrival time and vascular transit times, has been outlined in elegant detail in the literature (Hua et al., 2011a).

Finally, both VASO and iVASO acquisitions are fundamentally limited by the fact that, similar to BOLD, they do not provide a quantitative map but only a physiologically-weighted signal. Magnitude VASO and iVASO images are fundamentally T_1-weighted (and moderately T_2-weighted at 3.0T) images from which quantitative CBV information must be inferred by applying a model and assuming a baseline CBV. In more recent studies, iVASO experiments have been interleaved with images in which inflowing blood water is not

inverted, and the difference contains information on absolute arterial CBV (Figure 9). This so-called iVASO with dynamic subtraction (iVASO-DS) approach is similar in many ways to ASL in acquisition, as images with and without blood attenuation are interleaved, however the difference is that iVASO-DS acquires images prior to blood water exchange with tissue, whereas ASL acquires the images after (Donahue et al., 2010b; Hua et al., 2011b). The iVASO-DS theory has been outlined in detail (Hua et al., 2011b), and this method has been compared with more standard contrast-based CBV approaches in patients with arterial steno-occlusive disease (Donahue et al., 2010b). In principle, sequential ASL, iVASO-DS, and BOLD acquisition should allow for CBF, CBV, and blood oxygenation level to be extracted when all methods are applied with appropriate imaging parameters and postprocessing considerations.

Post-processing of VASO and iVASO functional data

Analyzing the VASO signal involves a similar range of steps as BOLD analysis, with several small exceptions. First, data are motion corrected. Algorithms optimized for motion correction of BOLD data perform well, and the same algorithms as described in the ASL section above can be applied. Second, the time course of the VASO signal is calculated. Similar to ASL, this can be achieved either in an anatomical region-of-interest or in voxels meeting statistical activation criteria. If statistical activation maps are of interest, general linear models can be applied, very similar to BOLD analysis, with the exception that activation for vasodilatory stimuli will reduce the signal. This is due to nulling of the blood water compartment which then expands during the functional stimulus and reduces the detectable extravascular water signal. Therefore, if t-statistics or z-statistics are calculated by comparing the data time course with a regressor, negative statistical thresholds should be evaluated for vasodilatory responses. The signal change is calculated by comparing the difference between the activated data points and the baseline data points, generally excluding at least one TR immediately after the onset and 2–3 TRs after cessation of the stimulus; this is to ensure that the signal has had sufficient time to either reach its activated or baseline level. At typical spatial resolutions available at 1.5T–3.0T (Figure 8), it is generally found that the CBV-weighted VASO signal increases slightly (1–3s) before the BOLD response, and for block stimuli of 20–40s, returns to baseline quickly (5–10s) after stimulus cessation, during the period of the BOLD post-stimulus undershoot (Donahue et al., 2009c; Hua et al., 2011c; Lu et al., 2004b). However, recent data in somatosensory and motor cortex of anesthetized rats have shown that the BOLD effect may increase much more quickly (e.g., < 1s) and varies with cortical depth (Yu et al., 2014); similar VASO experiments in animals at ultra high spatial resolution (approximately 0.5 mm in-plane) as well have shown faster CBV responses to stimulation that also vary with cortical depth (Huber et al., 2015b), and the BOLD return to baseline also may be cortically-dependent (Siero et al., 2015). Therefore, these trends may vary considerably depending on region considered and spatial resolution employed. Finally, this signal change can be converted to a CBV change using the equations outlined in the quantification section above.

Recently, very elegant work has demonstrated the potential of using VASO at the high field strength of 7.0T (Hua et al., 2013; Huber et al., 2014a; Huber et al., 2014b; Krieger et al., 2015), and new insights regarding neurovascular coupling and laminar hemodynamics have

been elucidated as a result of these data (Figure 10). Advantages of performing VASO at very high field strength relate to the higher SNR, but disadvantages are that BOLD effects will increase with field strength (Donahue et al., 2011; Duong et al., 2003). Therefore, even for relatively short TEs of 10 ms or less, the extravascular BOLD effect (increases in tissue water T_2* secondary to capillary and venous blood oxygenation increases) will confound and even overwhelm the negative vasodilatory VASO signal change. These BOLD effects are frequently ignored at 3.0T, as extravascular BOLD effects are 30–40% smaller at 3.0T relative to 7.0T, and at a short TE of 10 ms or less relatively small compared with the larger 1–5% VASO signal reduction. At 7.0T, it is possible to quantify these BOLD effects and simply factor this component out of the VASO signal equation (Huber et al., 2014b). The details of this procedure have been outlined in the literature (Huber et al., 2014a; Huber et al., 2014b), and must be incorporated if VASO is performed at very high field strength.

Concluding remarks

BOLD fMRI has transformed the field of human functional neuroimaging, largely due to its noninvasive nature and relative ease of implementation for functional mapping with good temporal resolution and spatial coverage. However, BOLD fMRI continues to suffer from multiple hemodynamic and metabolic contributions, which is why it remains largely qualitative in nature. CBF-weighted ASL and CBV-weighted VASO fMRI have emerged as alternatives to BOLD fMRI and are appealing due to their sensitivity to individual physiological parameters when appropriately implemented. These methods can also be performed quickly in sequence with BOLD and other methods for a more thorough understanding of cerebral physiology. The acquisition procedures for these methods have been outlined in detail in multiple reviews, however there are fewer succinct summaries of the relevant considerations and post-processing procedures that are necessary to responsibly analyze these data in *functional* experiments. This review is intended to provide such an overview and to outline the range of accepted procedures for quantifying CBF and CBV changes from these emerging alternative functional neuroimaging methods.

Acknowledgments

We would like to acknowledge the following sources of funding: NIH/NINDS 1R01NS07882801A1 (Donahue MJ), NIH/NINDS 1R01NS097763 (Donahue MJ), NIH/NINR 1R01NR01507901 (Donahue MJ), AHA Southeastern affiliate 14GRNT20150004 (Donahue MJ), AHA National affiliate 14CSA20380466 (Donahue MJ and Jordan L). We are also grateful to Drs. Laurentius Huber and Jun Hua for contributing figures for this article.

References

Adamson JW, Finch CA. Hemoglobin function, oxygen affinity, and erythropoietin. Annu Rev Physiol. 1975; 37:351–369. [PubMed: 235878]

Aguirre GK, Detre JA, Zarahn E, Alsop DC. Experimental design and the relative sensitivity of BOLD and perfusion fMRI. Neuroimage. 2002; 15:488–500. [PubMed: 11848692]

Alsop DC, Detre JA, Golay X, Gunther M, Hendrikse J, Hernandez-Garcia L, Lu H, Macintosh BJ, Parkes LM, Smits M, van Osch MJ, Wang DJ, Wong EC, Zaharchuk G. Recommended implementation of arterial spin-labeled perfusion MRI for clinical applications: A consensus of the ISMRM perfusion study group and the European consortium for ASL in dementia. Magn Reson Med. 2014 Jan; 73(1):102–116. 2015. [PubMed: 24715426]

Ances BM, Liang CL, Leontiev O, Perthen JE, Fleisher AS, Lansing AE, Buxton RB. Effects of aging on cerebral blood flow, oxygen metabolism, and blood oxygenation level dependent responses to visual stimulation. Hum Brain Mapp. 2009; 30:1120–1132. [PubMed: 18465743]

Aslan S, Xu F, Wang PL, Uh J, Yezhuvath US, van Osch M, Lu H. Estimation of labeling efficiency in pseudocontinuous arterial spin labeling. Magn Reson Med. 2010; 63:765–771. [PubMed: 20187183]

Beck, WS. Hematology. 5th. Cambridge, Mass: MIT Press; 1991.

Blicher JU, Stagg CJ, O'Shea J, Ostergaard L, MacIntosh BJ, Johansen-Berg H, Jezzard P, Donahue MJ. Visualization of altered neurovascular coupling in chronic stroke patients using multimodal functional MRI. J Cereb Blood Flow Metab. 2012; 32:2044–2054. [PubMed: 22828998]

Buxton RB, Uludag K, Dubowitz DJ, Liu TT. Modeling the hemodynamic response to brain activation. NeuroImage. 2004; 23(Suppl 1):S220–S233. [PubMed: 15501093]

Chen JJ, Wieckowska M, Meyer E, Pike GB. Cerebral blood flow measurement using fMRI and PET: a cross-validation study. Int J Biomed Imaging. 2008; 2008:516359. [PubMed: 18825270]

Cheng Y, van Zijl PC, Hua J. Measurement of parenchymal extravascular R2* and tissue oxygen extraction fraction using multi-echo vascular space occupancy MRI at 7 T. NMR Biomed. 2015; 28:264–271. [PubMed: 25521948]

Chiarelli PA, Bulte DP, Gallichan D, Piechnik SK, Wise R, Jezzard P. Flow-metabolism coupling in human visual, motor, and supplementary motor areas assessed by magnetic resonance imaging. Magn Reson Med. 2007; 57:538–547. [PubMed: 17326178]

Ciris PA, Qiu M, Constable RT. Noninvasive MRI measurement of the absolute cerebral blood volume-cerebral blood flow relationship during visual stimulation in healthy humans. Magn Reson Med. 2014; 72:864–875. [PubMed: 24151246]

Dai W, Garcia D, de Bazelaire C, Alsop DC. Continuous flow-driven inversion for arterial spin labeling using pulsed radio frequency and gradient fields. Magn Reson Med. 2008; 60:1488–1497. [PubMed: 19025913]

Davis TL, Kwong KK, Weisskoff RM, Rosen BR. Calibrated functional MRI: mapping the dynamics of oxidative metabolism. Proc Natl Acad Sci U S A. 1998; 95:1834–1839. [PubMed: 9465103]

Demirci O, Clark VP, Magnotta VA, Andreasen NC, Lauriello J, Kiehl KA, Pearlson GD, Calhoun VD. A Review of Challenges in the Use of fMRI for Disease Classification / Characterization and A Projection Pursuit Application from Multi-site fMRI Schizophrenia Study. Brain imaging and behavior. 2008; 2:147–226.

Derdeyn CP, Videen TO, Yundt KD, Fritsch SM, Carpenter DA, Grubb RL, Powers WJ. Variability of cerebral blood volume and oxygen extraction: stages of cerebral haemodynamic impairment revisited. Brain. 2002; 125:595–607. [PubMed: 11872616]

Detre JA, Leigh JS, Williams DS, Koretsky AP. Perfusion imaging. Magn Reson Med. 1992; 23:37–45. [PubMed: 1734182]

Detre JA, Wang J. Technical aspects and utility of fMRI using BOLD and ASL. Clin Neurophysiol. 2002; 113:621–634. [PubMed: 11976042]

Detre JA, Wang J, Wang Z, Rao H. Arterial spin-labeled perfusion MRI in basic and clinical neuroscience. Curr Opin Neurol. 2009; 22:348–355. [PubMed: 19491678]

Donahue MJ, Blicher JU, Ostergaard L, Feinberg DA, MacIntosh BJ, Miller KL, Gunther M, Jezzard P. Cerebral blood flow, blood volume, and oxygen metabolism dynamics in human visual and motor cortex as measured by whole-brain multi-modal magnetic resonance imaging. J Cereb Blood Flow Metab. 2009a; 29:1856–1866. [PubMed: 19654592]

Donahue MJ, Dethrage LM, Faraco CC, Jordan LC, Clemmons P, Singer R, Mocco J, Shyr Y, Desai A, O'Duffy A, Riebau D, Hermann L, Connors J, Kirshner H, Strother MK. Routine clinical evaluation of cerebrovascular reserve capacity using carbogen in patients with intracranial stenosis. Stroke. 2014a; 45:2335–2341. [PubMed: 24938845]

Donahue MJ, Faraco CC, Strother MK, Chappell MA, Rane S, Dethrage LM, Hendrikse J, Siero JC. Bolus arrival time and cerebral blood flow responses to hypercarbia. J Cereb Blood Flow Metab. 2014b; 34:1243–1252. [PubMed: 24780904]

Donahue MJ, Hoogduin H, Smith SM, Siero JC, Chappell M, Petridou N, Jezzard P, Luijten PR, Hendrikse J. Spontaneous blood oxygenation level-dependent fMRI signal is modulated by

behavioral state and correlates with evoked response in sensorimotor cortex: a 7.0-T fMRI study. Hum Brain Mapp. 2012a; 33:511–522. [PubMed: 21455940]

Donahue MJ, Hoogduin H, van Zijl PC, Jezzard P, Luijten PR, Hendrikse J. Blood oxygenation level-dependent (BOLD) total and extravascular signal changes and DeltaR2* in human visual cortex at 1.5, 3.0 and 7.0 T. NMR Biomed. 2011; 24:25–34. [PubMed: 21259367]

Donahue MJ, Hua J, Pekar JJ, van Zijl PC. Effect of inflow of fresh blood on vascular-space-occupancy (VASO) contrast. Magn Reson Med. 2009b; 61:473–480. [PubMed: 19161167]

Donahue MJ, Hussey E, Rane S, Wilson T, van Osch M, Hartkamp N, Hendrikse J, Ally BA. Vessel-encoded arterial spin labeling (VE-ASL) reveals elevated flow territory asymmetry in older adults with substandard verbal memory performance. J Magn Reson Imaging. 2014c; 39:377–386. [PubMed: 23633160]

Donahue MJ, Lu H, Jones CK, Edden RA, Pekar JJ, van Zijl PC. Theoretical and experimental investigation of the VASO contrast mechanism. Magn Reson Med. 2006; 56:1261–1273. [PubMed: 17075857]

Donahue MJ, Near J, Blicher JU, Jezzard P. Baseline GABA concentration and fMRI response. Neuroimage. 2010a; 53:392–398. [PubMed: 20633664]

Donahue MJ, Sideso E, MacIntosh BJ, Kennedy J, Handa A, Jezzard P. Absolute arterial cerebral blood volume quantification using inflow vascular-space-occupancy with dynamic subtraction magnetic resonance imaging. J Cereb Blood Flow Metab. 2010b; 30:1329–1342. [PubMed: 20145656]

Donahue MJ, Stevens RD, de Boorder M, Pekar JJ, Hendrikse J, van Zijl PC. Hemodynamic changes after visual stimulation and breath holding provide evidence for an uncoupling of cerebral blood flow and volume from oxygen metabolism. J Cereb Blood Flow Metab. 2009c; 29:176–185. [PubMed: 18797471]

Donahue MJ, Strother MK, Hendrikse J. Novel MRI approaches for assessing cerebral hemodynamics in ischemic cerebrovascular disease. Stroke. 2012b; 43:903–915. [PubMed: 22343644]

Duong TQ, Yacoub E, Adriany G, Hu X, Ugurbil K, Kim SG. Microvascular BOLD contribution at 4 and 7 T in the human brain: gradient-echo and spin-echo fMRI with suppression of blood effects. Magn Reson Med. 2003; 49:1019–1027. [PubMed: 12768579]

Eichling JO, Raichle ME, Grubb RL Jr, Larson KB, Ter-Pogossian MM. In vivo determination of cerebral blood volume with radioactive oxygen-15 in the monkey. Circ Res. 1975; 37:707–714. [PubMed: 811413]

Faraco CC, Strother MK, Dethrage LM, Jordan L, Singer R, Clemmons PF, Donahue MJ. Dual echo vessel-encoded ASL for simultaneous BOLD and CBF reactivity assessment in patients with ischemic cerebrovascular disease. Magn Reson Med. 2015a; 73:1579–1592. [PubMed: 24757044]

Faraco CC, Strother MK, Siero JC, Arteaga DF, Scott AO, Jordan LC, Donahue MJ. The cumulative influence of hyperoxia and hypercapnia on blood oxygenation and R. J Cereb Blood Flow Metab. 2015b Dec; 35(12):2032–2042. 2015. [PubMed: 26174329]

Fox MD, Raichle ME. Spontaneous fluctuations in brain activity observed with functional magnetic resonance imaging. Nat Rev Neurosci. 2007; 8:700–711. [PubMed: 17704812]

Frost R, Hess AT, Okell TW, Chappell MA, Tisdall MD, van der Kouwe AJ, Jezzard P. Prospective motion correction and selective reacquisition using volumetric navigators for vessel-encoded arterial spin labeling dynamic angiography. Magn Reson Med. 2015 [2015 Nov 14]

Gabr RE, Hasan KM, Haque ME, Nelson FM, Wolinsky JS, Narayana PA. Optimal combination of FLAIR and T2-weighted MRI for improved lesion contrast in multiple sclerosis. J Magn Reson Imaging. 2016 [2016 Apr 29]

Gonzalez-At JB, Alsop DC, Detre JA. Cerebral perfusion and arterial transit time changes during task activation determined with continuous arterial spin labeling. Magn Reson Med. 2000; 43:739–746. [PubMed: 10800040]

Grubb RL Jr, Raichle ME, Eichling JO, Ter-Pogossian MM. The effects of changes in PaCO2 on cerebral blood volume, blood flow, and vascular mean transit time. Stroke. 1974; 5:630–639. [PubMed: 4472361]

Grubb RL Jr, Raichle ME, Higgins CS, Eichling JO. Measurement of regional cerebral blood volume by emission tomography. Ann Neurol. 1978; 4:322–328. [PubMed: 727738]

Gu H, Stein EA, Yang Y. Nonlinear responses of cerebral blood volume, blood flow and blood oxygenation signals during visual stimulation. Magn Reson Imaging. 2005; 23:921–928. [PubMed: 16310107]

Guidi M, Huber L, Lampe L, Gauthier CJ, Moller HE. Lamina-dependent calibrated BOLD response in human primary motor cortex. Neuroimage. 2016; 141:250–261. [PubMed: 27364473]

Gunther M, Oshio K, Feinberg DA. Single-shot 3D imaging techniques improve arterial spin labeling perfusion measurements. Magn Reson Med. 2005; 54:491–498. [PubMed: 16032686]

Guyton, AC. Basic human physiology: normal function and mechanisms of disease. 2d. Philadelphia: Saunders; 1977.

Hendrikse J, van der Zwan A, Ramos LM, van Osch MJ, Golay X, Tulleken CA, van der Grond J. Altered flow territories after extracranial-intracranial bypass surgery. Neurosurgery. 2005; 57:486–494. [PubMed: 16145527]

Hennig J, Speck O, Koch MA, Weiller C. Functional magnetic resonance imaging: a review of methodological aspects and clinical applications. J Magn Reson Imaging. 2003; 18:1–15. [PubMed: 12815634]

Herold S, Brozovic M, Gibbs J, Lammertsma AA, Leenders KL, Carr D, Fleming JS, Jones T. Measurement of regional cerebral blood flow, blood volume and oxygen metabolism in patients with sickle cell disease using positron emission tomography. Stroke. 1986; 17:692–698. [PubMed: 3488606]

Herscovitch P, Raichle ME. What is the correct value for the brain--blood partition coefficient for water? J Cereb Blood Flow Metab. 1985; 5:65–69. [PubMed: 3871783]

Hua J, Donahue MJ, Zhao JM, Grgac K, Huang AJ, Zhou J, van Zijl PC. Magnetization transfer enhanced vascular-space-occupancy (MT-VASO) functional MRI. Magn Reson Med. 2009; 61:944–951. [PubMed: 19215043]

Hua J, Jones CK, Qin Q, van Zijl PC. Implementation of vascular-space-occupancy MRI at 7T. Magn Reson Med. 2013; 69:1003–1013. [PubMed: 22585570]

Hua J, Qin Q, Donahue MJ, Zhou J, Pekar JJ, van Zijl PC. Inflow-based vascular-space-occupancy (iVASO) MRI. Magn Reson Med. 2011a; 66:40–56. [PubMed: 21695719]

Hua J, Qin Q, Pekar JJ, van Zijl PC. Measurement of absolute arterial cerebral blood volume in human brain without using a contrast agent. NMR Biomed. 2011b; 24:1313–1325. [PubMed: 21608057]

Hua J, Stevens RD, Huang AJ, Pekar JJ, van Zijl PC. Physiological origin for the BOLD poststimulus undershoot in human brain: vascular compliance versus oxygen metabolism. J Cereb Blood Flow Metab. 2011c; 31:1599–1611. [PubMed: 21468090]

Huber, L., Goense, J., Kennerley, A., Guidi, M., Trampel, R., Turner, R., Moller, HE. Micro- And Macrovascular Contributions to Layer-Dependent Blood Volume FMRI: A Multi-Modal, Multi-Species Comparison. 23rd Annual International Society for Magnetic Resonance in Medicine; Toronto, Canada. 2015a. Abstract 317

Huber L, Goense J, Kennerley AJ, Ivanov D, Krieger SN, Lepsien J, Trampel R, Turner R, Moller HE. Investigation of the neurovascular coupling in positive and negative BOLD responses in human brain at 7 T. Neuroimage. 2014a; 97:349–362. [PubMed: 24742920]

Huber L, Goense J, Kennerley AJ, Trampel R, Guidi M, Reimer E, Ivanov D, Neef N, Gauthier CJ, Turner R, Moller HE. Cortical lamina-dependent blood volume changes in human brain at 7 T. Neuroimage. 2015b; 107:23–33. [PubMed: 25479018]

Huber L, Ivanov D, Guidi M, Turner R, Uludag K, Moller HE, Poser BA. Functional cerebral blood volume mapping with simultaneous multi-slice acquisition. Neuroimage. 2016a; 125:1159–1168. [PubMed: 26522423]

Huber L, Ivanov D, Krieger SN, Streicher MN, Mildner T, Poser BA, Moller HE, Turner R. Slab-selective, BOLD-corrected VASO at 7 Tesla provides measures of cerebral blood volume reactivity with high signal-to-noise ratio. Magn Reson Med. 2014b; 72:137–148. [PubMed: 23963641]

Huber, L., Ivanov, D., Marrett, S., Panwar, P., Uludag, K., Bandettini, P., Poser, BA. Blood Volume FMRI with 3D-EPI-VASO: Any Benefits Over SMS-VASO?. 24th Annual International Society for Magnetic Resonance in Medicine; Singapore, Singapore. 2016b. Abstract 944

Jenkinson M, Bannister P, Brady M, Smith S. Improved optimization for the robust and accurate linear registration and motion correction of brain images. Neuroimage. 2002; 17:825–841. [PubMed: 12377157]

Jezzard P, Buxton RB. The clinical potential of functional magnetic resonance imaging. J Magn Reson Imaging. 2006; 23:787–793. [PubMed: 16649209]

Jin T, Kim SG. Spatial dependence of CBV-fMRI: a comparison between VASO and contrast agent based methods. Conf Proc IEEE Eng Med Biol Soc. 2006; 1:25–28. [PubMed: 17946773]

Jordan LC, Gindville MC, Scott AO, Juttukonda MR, Strother MK, Kassim AA, Chen SC, Lu H, Pruthi S, Shyr Y, Donahue MJ. Non-invasive imaging of oxygen extraction fraction in adults with sickle cell anaemia. Brain. 2016 Mar; 139(Pt 3):738–750. 2016. [PubMed: 26823369]

Kannurpatti SS, Motes MA, Rypma B, Biswal BB. Non-neural BOLD variability in block and event-related paradigms. Magn Reson Imaging. 2011; 29:140–146. [PubMed: 20833501]

Kim DS, Ronen I, Olman C, Kim SG, Ugurbil K, Toth LJ. Spatial relationship between neuronal activity and BOLD functional MRI. Neuroimage. 2004; 21:876–885. [PubMed: 15006654]

Kim SG, Harel N, Jin T, Kim T, Lee P, Zhao F. Cerebral blood volume MRI with intravascular superparamagnetic iron oxide nanoparticles. NMR Biomed. 2013; 26:949–962. [PubMed: 23208650]

Kim YR, Huang IJ, Lee SR, Tejima E, Mandeville JB, van Meer MP, Dai G, Choi YW, Dijkhuizen RM, Lo EH, Rosen BR. Measurements of BOLD/CBV ratio show altered fMRI hemodynamics during stroke recovery in rats. J Cereb Blood Flow Metab. 2005; 25:820–829. [PubMed: 15758949]

Krieger SN, Huber L, Poser BA, Turner R, Egan GF. Simultaneous acquisition of cerebral blood volume-, blood flow-, and blood oxygenation-weighted MRI signals at ultra-high magnetic field. Magn Reson Med. 2015; 74:513–517. [PubMed: 25195774]

Li X, Branch CA, Ardekani BA, Bertisch H, Hicks C, DeLisi LE. fMRI study of language activation in schizophrenia, schizoaffective disorder and in individuals genetically at high risk. Schizophrenia research. 2007; 96:14–24. [PubMed: 17719745]

Liu P, Lu H, Filbey FM, Pinkham AE, McAdams CJ, Adinoff B, Daliparthi V, Cao Y. Automatic and reproducible positioning of phase-contrast MRI for the quantification of global cerebral blood flow. PLoS One. 2014; 9:e95721. [PubMed: 24787742]

Lu, H. Magnetization “Reset” for Non-Steady-State Blood Spins in Vascular-Space-Occupancy (VASO) fMRI. 16th Annual International Society for Magnetic Resonance in Medicine; Toronto, Canada. 2008. Abstract 406

Lu H, Clingman C, Golay X, van Zijl PC. Determining the longitudinal relaxation time (T1) of blood at 3.0 Tesla. Magn Reson Med. 2004a; 52:679–682. [PubMed: 15334591]

Lu H, Donahue MJ, van Zijl PC. Detrimental effects of BOLD signal in arterial spin labeling fMRI at high field strength. Magn Reson Med. 2006; 56:546–552. [PubMed: 16894581]

Lu HH, Golay X, Pekar JJ, Van Zijl PC. Functional magnetic resonance imaging based on changes in vascular space occupancy. Magn Reson Med. 2003; 50:263–274. [PubMed: 12876702]

Lu H, Golay X, Pekar JJ, Van Zijl PC. Sustained poststimulus elevation in cerebral oxygen utilization after vascular recovery. J Cereb Blood Flow Metab. 2004b; 24:764–770. [PubMed: 15241184]

Lu H, Golay X, van Zijl PC. Intervoxel heterogeneity of event-related functional magnetic resonance imaging responses as a function of T(1) weighting. Neuroimage. 2002; 17:943–955. [PubMed: 12377168]

Lu H, Nagae-Poetscher LM, Golay X, Lin D, Pomper M, van Zijl PC. Routine clinical brain MRI sequences for use at 3.0 Tesla. J Magn Reson Imaging. 2005; 22:13–22. [PubMed: 15971174]

Lu H, van Zijl PC. A review of the development of Vascular-Space-Occupancy (VASO) fMRI. Neuroimage. 2012; 62:736–742. [PubMed: 22245650]

Lu H, van Zijl PC, Hendrikse J, Golay X. Multiple acquisitions with global inversion cycling (MAGIC): a multislice technique for vascular-space-occupancy dependent fMRI. Magn Reson Med. 2004c; 51:9–15. [PubMed: 14705039]

Lu H, Xu F, Rodrigue KM, Kennedy KM, Cheng Y, Flicker B, Hebrank AC, Uh J, Park DC. Alterations in cerebral metabolic rate and blood supply across the adult lifespan. Cereb Cortex. 2011; 21:1426–1434. [PubMed: 21051551]

Lu H, Yezhuvath US, Xiao G. Improving fMRI sensitivity by normalization of basal physiologic state. Hum Brain Mapp. 2010; 31:80–87. [PubMed: 19585589]

MacIntosh BJ, Filippini N, Chappell MA, Woolrich MW, Mackay CE, Jezzard P. Assessment of arterial arrival times derived from multiple inversion time pulsed arterial spin labeling MRI. Magn Reson Med. 2010; 63:641–647. [PubMed: 20146233]

Maeda Y, Kudomi N, Sasakawa Y, Monden T, Kato K, Yamamoto Y, Kawai N, Nishiyama Y. Applicability of emission-based attenuation map for rapid CBF, OEF, and CMRO2 measurements using gaseous (15)O-labeled compounds. EJNMMI Phys. 2015; 2:12. [PubMed: 26501813]

Mani S, Pauly J, Conolly S, Meyer C, Nishimura D. Background suppression with multiple inversion recovery nulling: applications to projective angiography. Magn Reson Med. 1997; 37:898–905. [PubMed: 9178242]

Martuzzi R, Ramani R, Qiu M, Rajeevan N, Constable RT. Functional connectivity and alterations in baseline brain state in humans. NeuroImage. 2010; 49:823–834. [PubMed: 19631277]

Mildner T, Muller K, Hetzer S, Trampel R, Driesel W, Moller HE. Mapping of arterial transit time by intravascular signal selection. NMR Biomed. 2014; 27:594–609. [PubMed: 24610794]

Ogawa S, Lee TM, Kay AR, Tank DW. Brain magnetic resonance imaging with contrast dependent on blood oxygenation. Proc Natl Acad Sci U S A. 1990; 87:9868–9872. [PubMed: 2124706]

Okell TW, Chappell MA, Kelly ME, Jezzard P. Cerebral blood flow quantification using vessel-encoded arterial spin labeling. J Cereb Blood Flow Metab. 2013; 33:1716–1724. [PubMed: 23921895]

Perlmutter JS, Powers WJ, Herscovitch P, Fox PT, Raichle ME. Regional asymmetries of cerebral blood flow, blood volume, and oxygen utilization and extraction in normal subjects. J Cereb Blood Flow Metab. 1987; 7:64–67. [PubMed: 3492507]

Petersen ET, Mouridsen K, Golay X. all named co-authors of the Q.t.-r.s. The QUASAR reproducibility study, Part II. Results from a multi-center Arterial Spin Labeling test-retest study. Neuroimage. 2010; 49:104–113. [PubMed: 19660557]

Piechnik SK, Chiarelli PA, Jezzard P. Modelling vascular reactivity to investigate the basis of the relationship between cerebral blood volume and flow under CO2 manipulation. Neuroimage. 2008; 39:107–118. [PubMed: 17920935]

Poser BA, Norris DG. 3D single-shot VASO using a Maxwell gradient compensated GRASE sequence. Magn Reson Med. 2009; 62:255–262. [PubMed: 19319900]

Powers WJ, Grubb RL Jr, Darriet D, Raichle ME. Cerebral blood flow and cerebral metabolic rate of oxygen requirements for cerebral function and viability in humans. J Cereb Blood Flow Metab. 1985; 5:600–608. [PubMed: 3877067]

Rane S, Talati P, Donahue MJ, Heckers S. Inflow-vascular space occupancy (iVASO) reproducibility in the hippocampus and cortex at different blood water nulling times. Magn Reson Med. 2016; 75:2379–2387. [PubMed: 26192478]

Rogers BP, Avery SN, Heckers S. Internal representation of hierarchical sequences involves the default network. BMC Neurosci. 2010; 11:54. [PubMed: 20423509]

Scouten A, Constable RT. Applications and limitations of whole-brain MAGIC VASO functional imaging. Magn Reson Med. 2007; 58:306–315. [PubMed: 17654574]

Scouten A, Constable RT. VASO-based calculations of CBV change: accounting for the dynamic CSF volume. Magn Reson Med. 2008; 59:308–315. [PubMed: 18228581]

Seidel E, Eicke BM, Tettenborn B, Krummenauer F. Reference values for vertebral artery flow volume by duplex sonography in young and elderly adults. Stroke. 1999; 30:2692–2696. [PubMed: 10582999]

Siero JC, Hendrikse J, Hoogduin H, Petridou N, Luijten P, Donahue MJ. Cortical depth dependence of the BOLD initial dip and poststimulus undershoot in human visual cortex at 7 Tesla. Magn Reson Med. 2015; 73:2283–2295. [PubMed: 24989338]

Smith JF, Pillai A, Chen K, Horwitz B. Identification and validation of effective connectivity networks in functional magnetic resonance imaging using switching linear dynamic systems. Neuroimage. 2010; 52:1027–1040. [PubMed: 19969092]

Stefanovic B, Pike GB. Venous refocusing for volume estimation: VERVE functional magnetic resonance imaging. Magn Reson Med. 2005; 53:339–347. [PubMed: 15678548]

Tanenbaum AB, Snyder AZ, Brier MR, Ances BM. A method for reducing the effects of motion contamination in arterial spin labeling magnetic resonance imaging. J Cereb Blood Flow Metab. 2015; 35:1697–1702. [PubMed: 26036937]

Uh J, Lin AL, Lee K, Liu P, Fox P, Lu H. Validation of VASO cerebral blood volume measurement with positron emission tomography. Magn Reson Med. 2010 Mar; 65(3):744–749. 2011. [PubMed: 21337407]

van Osch MJ, Teeuwisse WM, van Walderveen MA, Hendrikse J, Kies DA, van Buchem MA. Can arterial spin labeling detect white matter perfusion signal? Magn Reson Med. 2009; 62:165–173. [PubMed: 19365865]

van Zijl PC, Eleff SM, Ulatowski JA, Oja JM, Ulug AM, Traystman RJ, Kauppinen RA. Quantitative assessment of blood flow, blood volume and blood oxygenation effects in functional magnetic resonance imaging. Nat Med. 1998; 4:159–167. [PubMed: 9461188]

Wang J, Alsop DC, Li L, Listerud J, Gonzalez-At JB, Schnall MD, Detre JA. Comparison of quantitative perfusion imaging using arterial spin labeling at 1.5 and 4.0 Tesla. Magn Reson Med. 2002; 48:242–254. [PubMed: 12210932]

Warmuth C, Gunther M, Zimmer C. Quantification of blood flow in brain tumors: comparison of arterial spin labeling and dynamic susceptibility-weighted contrast-enhanced MR imaging. Radiology. 2003; 228:523–532. [PubMed: 12819338]

Williams DS, Detre JA, Leigh JS, Koretsky AP. Magnetic resonance imaging of perfusion using spin inversion of arterial water. Proc Natl Acad Sci U S A. 1992; 89:212–216. [PubMed: 1729691]

Wong EC, Buxton RB, Frank LR. Implementation of quantitative perfusion imaging techniques for functional brain mapping using pulsed arterial spin labeling. NMR Biomed. 1997; 10:237–249. [PubMed: 9430354]

Wong EC, Buxton RB, Frank LR. Quantitative imaging of perfusion using a single subtraction (QUIPSS and QUIPSS II). Magn Reson Med. 1998; 39:702–708. [PubMed: 9581600]

Wu CW, Liu HL, Chen JH, Yang Y. Effects of CBV, CBF, and blood-brain barrier permeability on accuracy of PASL and VASO measurement. Magn Reson Med. 2010; 63:601–608. [PubMed: 20146228]

Ye FQ, Frank JA, Weinberger DR, McLaughlin AC. Noise reduction in 3D perfusion imaging by attenuating the static signal in arterial spin tagging (ASSIST). Magn Reson Med. 2000; 44:92–100. [PubMed: 10893526]

Yu X, Qian C, Chen DY, Dodd SJ, Koretsky AP. Deciphering laminar-specific neural inputs with line-scanning fMRI. Nat Methods. 2014; 11:55–58. [PubMed: 24240320]

Zaharchuk G, Do HM, Marks MP, Rosenberg J, Moseley ME, Steinberg GK. Arterial spin-labeling MRI can identify the presence and intensity of collateral perfusion in patients with moyamoya disease. Stroke. 2011; 42:2485–2491. [PubMed: 21799169]

Zhang D, Raichle ME. Disease and the brain's dark energy. Nat Rev Neurol. 2010; 6:15–28. [PubMed: 20057496]

Zhang Y, Brady M, Smith S. Segmentation of brain MR images through a hidden Markov random field model and the expectation-maximization algorithm. IEEE Trans Med Imaging. 2001; 20:45–57. [PubMed: 11293691]

Zhao JM, Clingman CS, Narvainen MJ, Kauppinen RA, van Zijl PC. Oxygenation and hematocrit dependence of transverse relaxation rates of blood at 3T. Magn Reson Med. 2007; 58:592–597. [PubMed: 17763354]

Zhou J, Wilson DA, Ulatowski JA, Traystman RJ, van Zijl PC. Two-compartment exchange model for perfusion quantification using arterial spin tagging. J Cereb Blood Flow Metab. 2001; 21:440–455. [PubMed: 11323530]

Zun Z, Shankaranarayanan A, Zaharchuk G. Pseudocontinuous arterial spin labeling with prospective motion correction (PCASL-PROMO). Magn Reson Med. 2014; 72:1049–1056. [PubMed: 24243585]

Highlights

- Review of basic physiology of cerebral blood flow and volume regulation
- Range of acquisitions and processing procedures for cerebral blood flow functional imaging
- Range of acquisitions and processing procedures for cerebral blood volume functional imaging
- Summary of parameters used for cerebral blood flow and volume quantification models

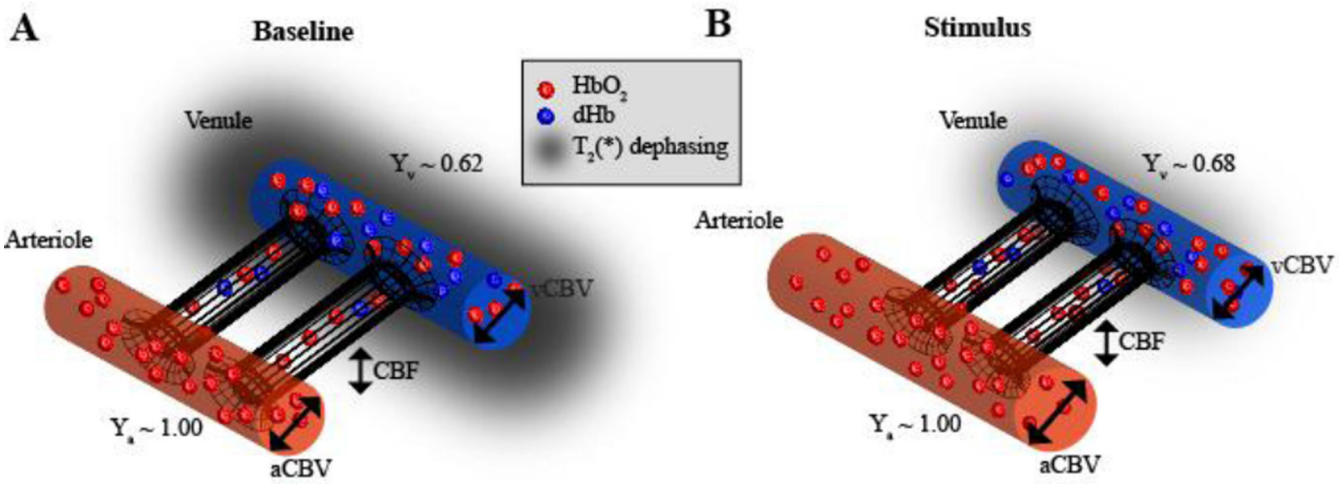

Figure 1. Physiology of blood oxygenation level-dependent (BOLD) functional magnetic resonance imaging (fMRI)

Blood is delivered to brain tissue from the arteries nearly 100% oxygenated (Y_a=1.00), after which restricted exchange occurs in the capillary bed, where oxygen and glucose move into the tissue and waste products such as CO_2 move from the tissue to the blood compartment and flow out through the venous system. The cerebral blood flow (CBF) describes the rate that the blood water is delivered to the tissue (ml blood / 100g tissue / minute), whereas the cerebral blood volume (CBV) describes the fraction of blood in a given brain region per unit brain volume (ml blood / ml parenchyma). Here both arterial (aCBV) and venous (vCBV) CBV are depicted. At baseline, on average an oxygen extraction fraction (OEF) of 30–40% leads to a venous blood oxygenation level (Y_v) of 60–70% in healthy brain. During periods of elevated neuronal activity, the cerebral metabolic rate of oxygen ($CMRO_2$) increase is outweighed by the CBF increase, leading to a slight elevation of Y_v. As oxyhemoglobin is diamagnetic (induces only a small magnetic field in the presence of an external field, B_0) and deoxyhemoglobin is paramagnetic (induces a larger local magnetic field in the presence of B_0), this fractional increase in Y_v leads to a lengthening of blood water and surrounding tissue water T_2(*), thereby increasing the MRI signal, a phenomenon known as the BOLD effect. Importantly, the BOLD effect depends on multiple hemodynamic and metabolic parameters (e.g., OEF, CBF, CBV, and $CMRO_2$), and therefore quantitative functional imaging frequently requires additional measurements of these parameters using alternative fMRI approaches.

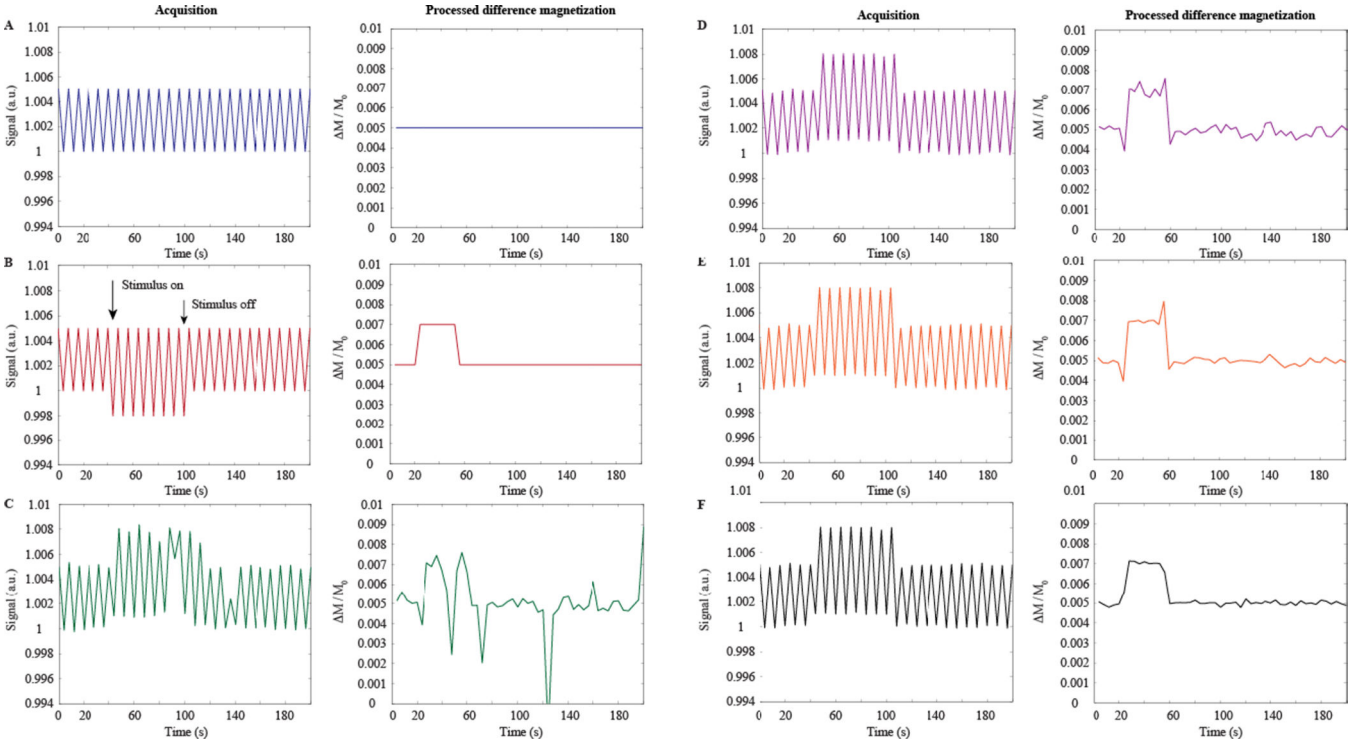

Figure 2. Salient arterial spin labeling (ASL) post-processing steps for simulated data, shown here for a pseudo-continuous ASL labeling scheme

For each panel (A–F), the left plot shows sequentially acquired control and label data, whereas the right panel shows subtracted data (e.g., control – label unless otherwise stated normalized by the equilibrium magnetization: $\Delta M/M_0$). (A) Sequentially-acquired control and label ASL scans demonstrate that at typical CBF levels, the label acquisition is approximately 0.5% less than the control acquisition, however the absolute difference may vary between approximately 0.25% and 2% depending on the ASL acquisition used and level of perfusion. In the absence of a stimulus, the difference magnetization acquired from pair-wise subtraction is stable and unchanging. (B) In the presence of a vasodilatory stimulus, the CBF will increase, thereby attenuating the label image further, and a resulting increase in $\Delta M/M_0$ is observed during the stimulus, which scales with the degree of hyperemia. (C) A more realistic time course, which contains contributions from motion, thermal and physiological noise, and blood oxygenation changes. Motion manifests as large increases or decreases in the signal; noise as temporal signal variations due to cardiac or respiratory fluctuations (<1 Hz), as well as thermal noise; and blood oxygenation changes as increases in both the control and label signal intensity due to $T_2^{(*)}$ reductions. (D) The data from (C) following motion correction, which reduces the largest fluctuations in the time course. (E) If the experiment is repeated, noise contributions will reduce upon averaging (shown here for five averages). (F) Large signal transitions near the onset and cessation of the stimulus are due to transient blood oxygenation differences between control and label pairs. When a surround subtraction approach is applied, these errors are reduced. The fully-processed (motion, block-averaged, and BOLD-corrected) time course in (F) closely resembles the ideal time course in (B).

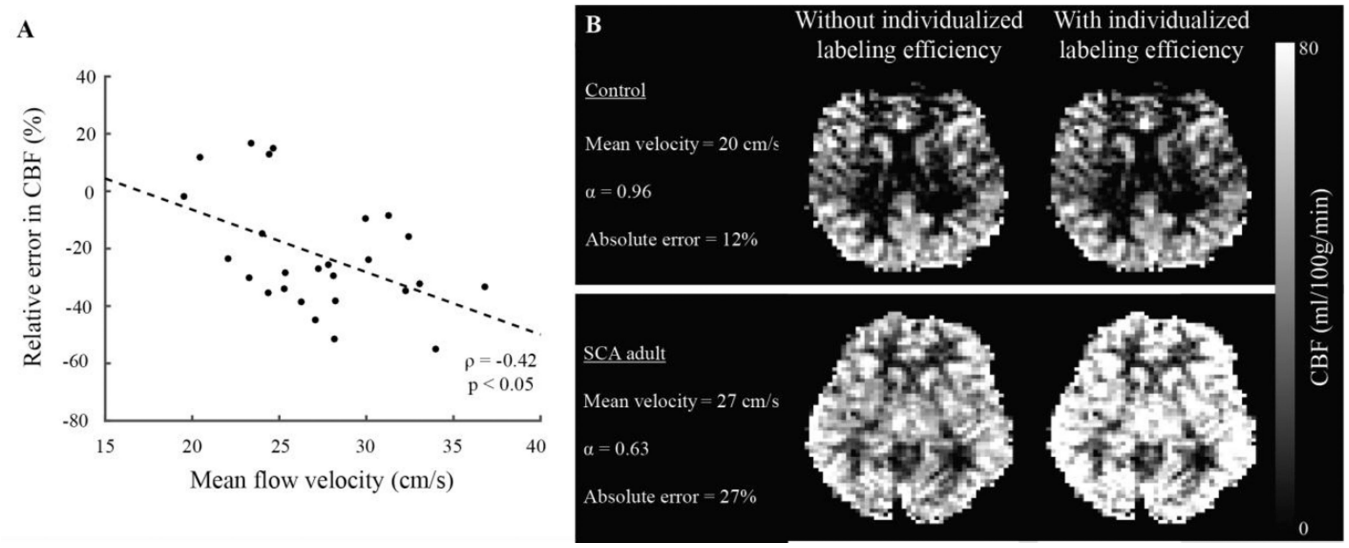

Figure 3. Effect of changes in cervical flow velocity on pseudo-continuous arterial spin labeling (pCASL) labeling efficiency and quantified cerebral blood flow (CBF)

Typical pCASL labeling pulse trains are optimized for a healthy range of mean (over diastole and systole) cervical velocities. However, in pathology (e.g., internal carotid artery stenosis, altered cardiac output, etc.) or in response to pharmaceutical or even strong neuronal challenges, these velocities may change. This will influence both the bolus arrival time (e.g., Figure 5) but also the pCASL labeling efficiency. (A) How the relative error (difference between true and measured CBF) changes with increasing mean cervical flow velocity, along with subjects with healthy (B) and (C) elevated mean cervical flow velocity secondary to elevated cardiac output.

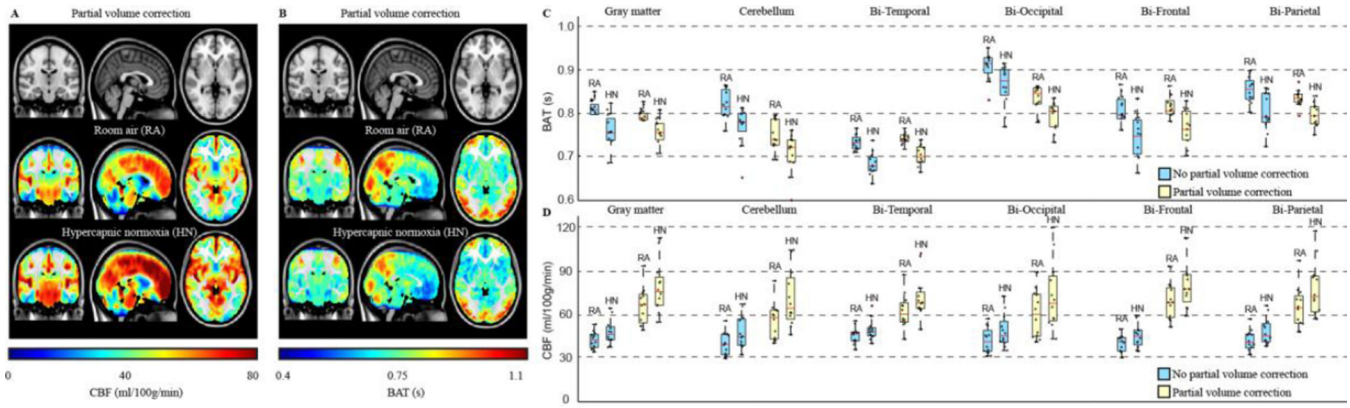

Figure 4. Functional cerebral blood flow (CBF) and bolus arrival time (BAT) values at baseline and in response to a mild vascular stimulus of hypercapnic normoxia (5% CO_2 / 21% O_2 / 74% N_2)

(A–B) CBF and BAT maps from 12 healthy adults show increases in CBF and decreases in BAT during the vascular stimulus. The changes are regionally-dependent (C–D), with CBF values in gray matter being larger and BAT values smaller after correction for partial volume contributions (white matter and CSF). Additional information on these values can be found in (Donahue et al., 2014b) and references therein.

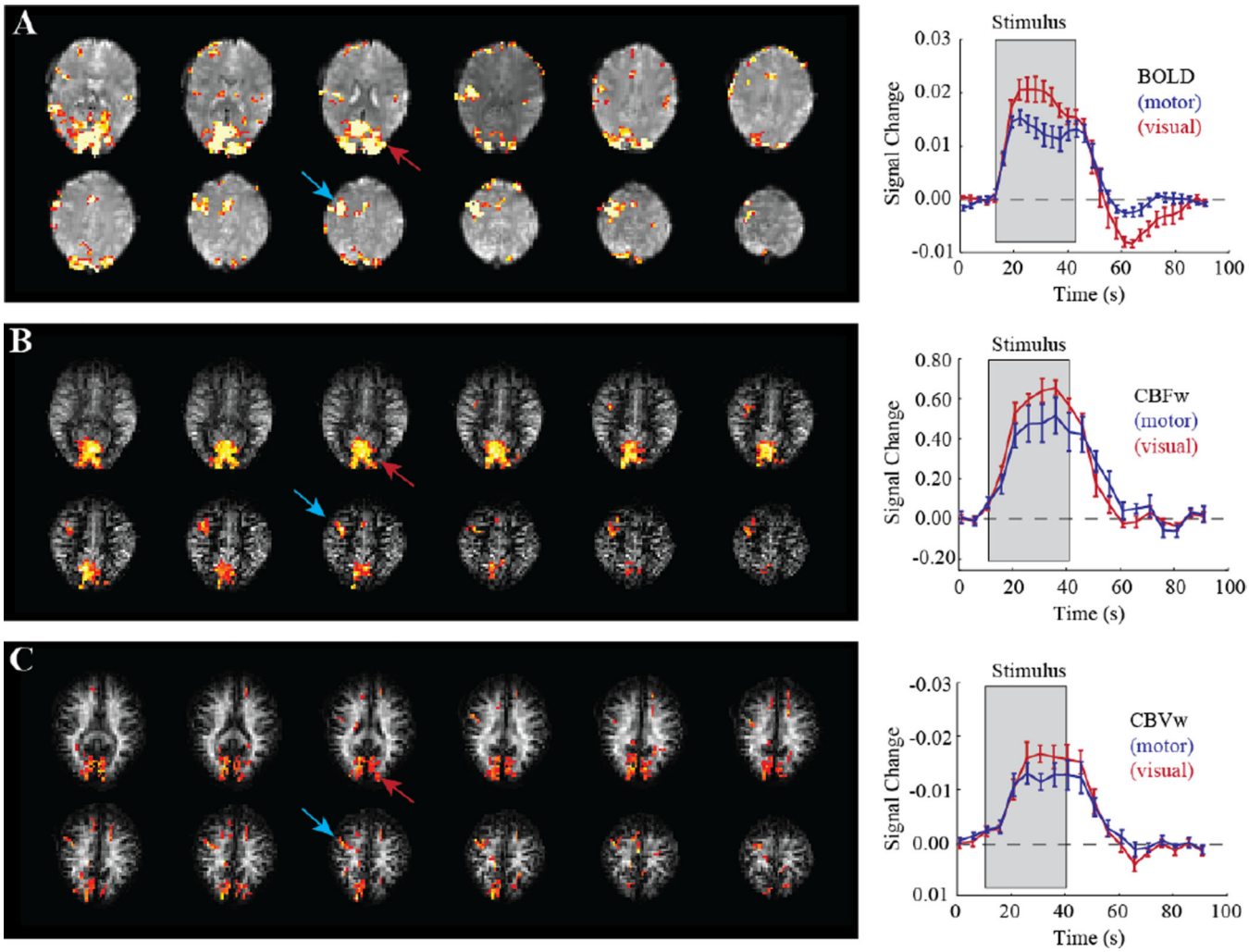

Figure 5. Multi-modal functional MRI (fMRI) with (A) qualitative blood oxygenation level-dependent (BOLD), (B) cerebral blood flow (CBF)-weighted (CBFw) ASL, and (C) cerebral blood volume (CBV)-weighted (CBVw) VASO

Images are from a single subject performing simultaneous visual stimulation (flashing blue/yellow checkerboard at 8 Hz) and right-handed joystick movement at a frequency of 1 Hz. Activation in visual cortex (red) and motor cortex (blue) is discernable in all imaging modalities; the corresponding time courses allow for interrogation of the temporal and quantitative hemodynamic properties of the brain response to these stimuli. The clinical relevance of such multimodal imaging is shown in Figure 6. Additional information on these signal characteristics at 3.0T can be found in (Donahue et al., 2009a; Hua et al., 2011c; Lu et al., 2004b)

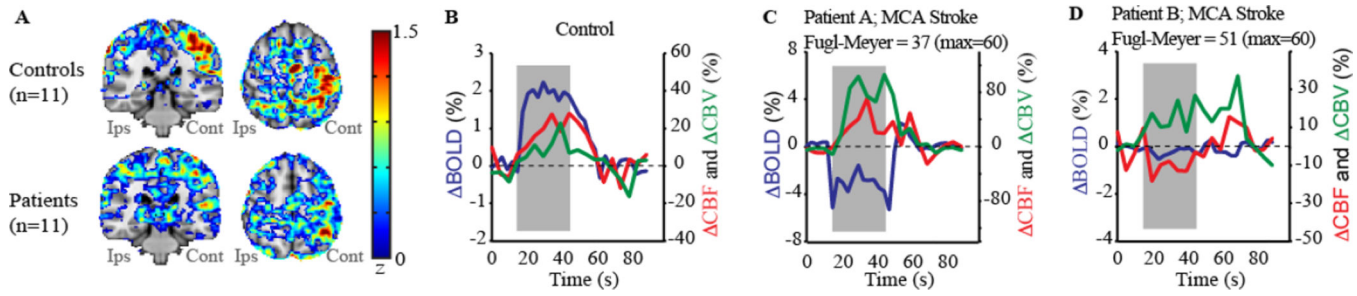

Figure 6. Data showing the potential utility of multi-modal quantitative functional neuroimaging for detecting altered hemodynamic relationships following stroke

(A) Activation maps in response to a unilateral joystick task for controls (n=11) and chronic stroke patients (n=11) following middle cerebral artery (MCA) territory ischemic stroke. In controls, activation is largest in the hemisphere contralateral (cont) to the moved hand; in patients movement always occurred with the paretic hand, yet activation is less well localized to primary motor cortex, consistent with remapping of motor function to new cortical regions. A block-averaged time course for (B) a control subject and (C–D) two different chronic MCA-territory stroke patients. Gray areas depict the stimulus period. For the control, a robust BOLD change ($P<0.05$) is observed with normal cerebral blood flow-weighted (CBFw) ($P<0.05$) and cerebral blood volume-weighted (CBVw) ($P<0.05$) reactivity. Alternatively, despite similar stroke types (right MCA territory; residual bilateral steno-occlusion), Patient A (Fugl-Meyer=37) is less-impaired than Patient B (Fugl-Meyer=51). In Patient A, CBF reactivity is maintained throughout motor cortex (red curve) by large autoregulatory increases in CBV (green curve), but negligible CBF reactivity is observed in Patient B. The BOLD response, which is negative or negligible in both patients, cannot explain the differences in motor function. Data demonstrate how multi-modal imaging can be used to explain differences in motor impairment for similar stroke extensions. Additional information in a larger patient cohort can be found in (Blicher et al., 2012).

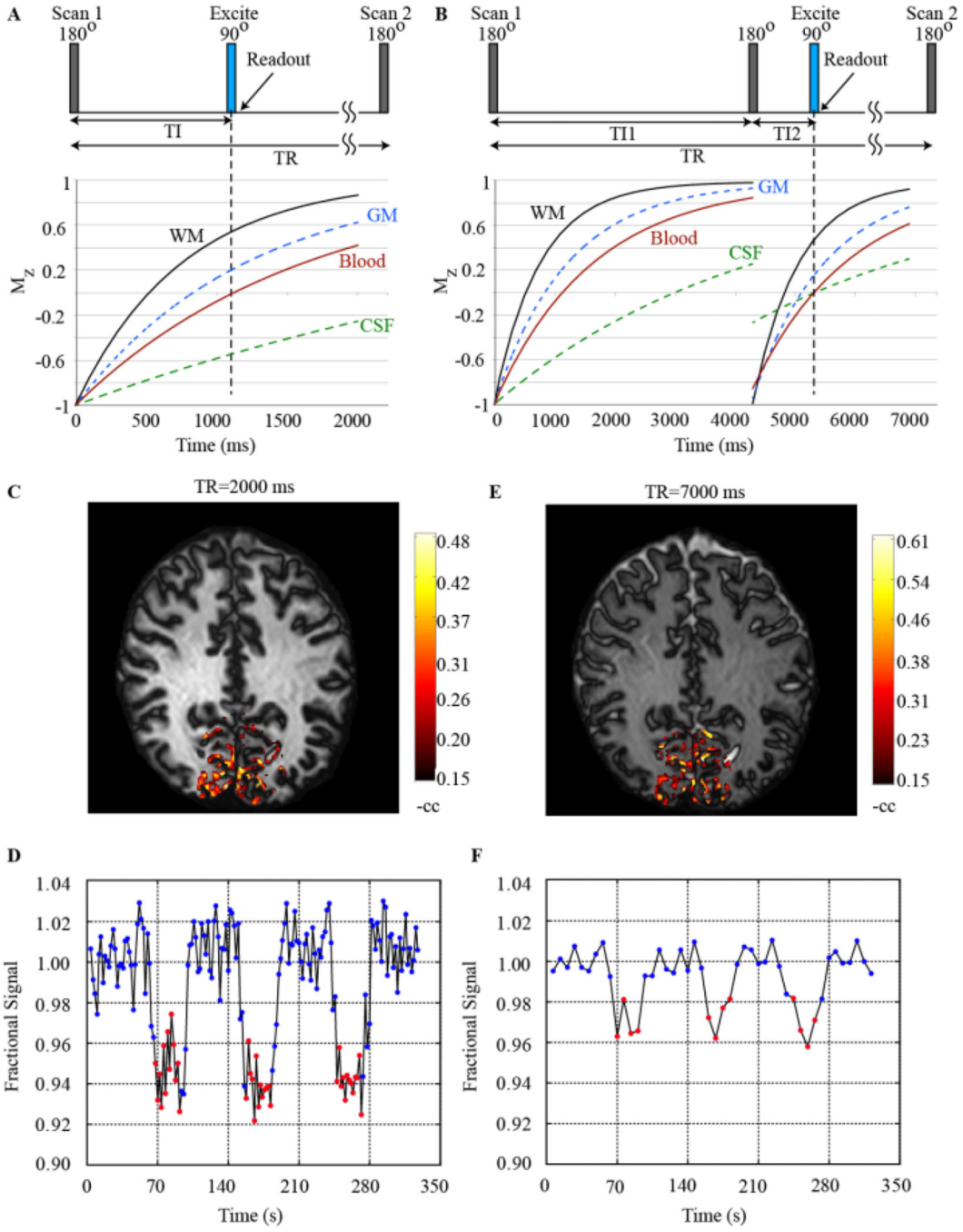

Figure 7. Principles of vascular space occupancy (VASO) functional MRI (fMRI)

(A) In conventional VASO, following a non-selective inversion, an image is acquired when the blood water signal is nulled, but the residual gray matter (GM), white matter (WM), and cerebrospinal fluid (CSF) signal is positive (owing to differing T_1; Table 1). (B) An additional inversion pulse can be added to simultaneously null the CSF signal in VASO-FLAIR. (C–D) Short TR VASO fMRI during a flashing checkerboard stimulus shows limited CSF signal and large negative signal changes. (E–F) Long TR VASO shows much higher residual CSF signal and smaller signal changes. Both blood inflow effects and partial

volume effects can be considered in cerebral blood volume (CBV) quantification models. Additional information on VASO and VASO-FLAIR implementation can be found in (Donahue et al., 2006; Huber et al., 2016a; Lu et al., 2003; Poser and Norris, 2009).

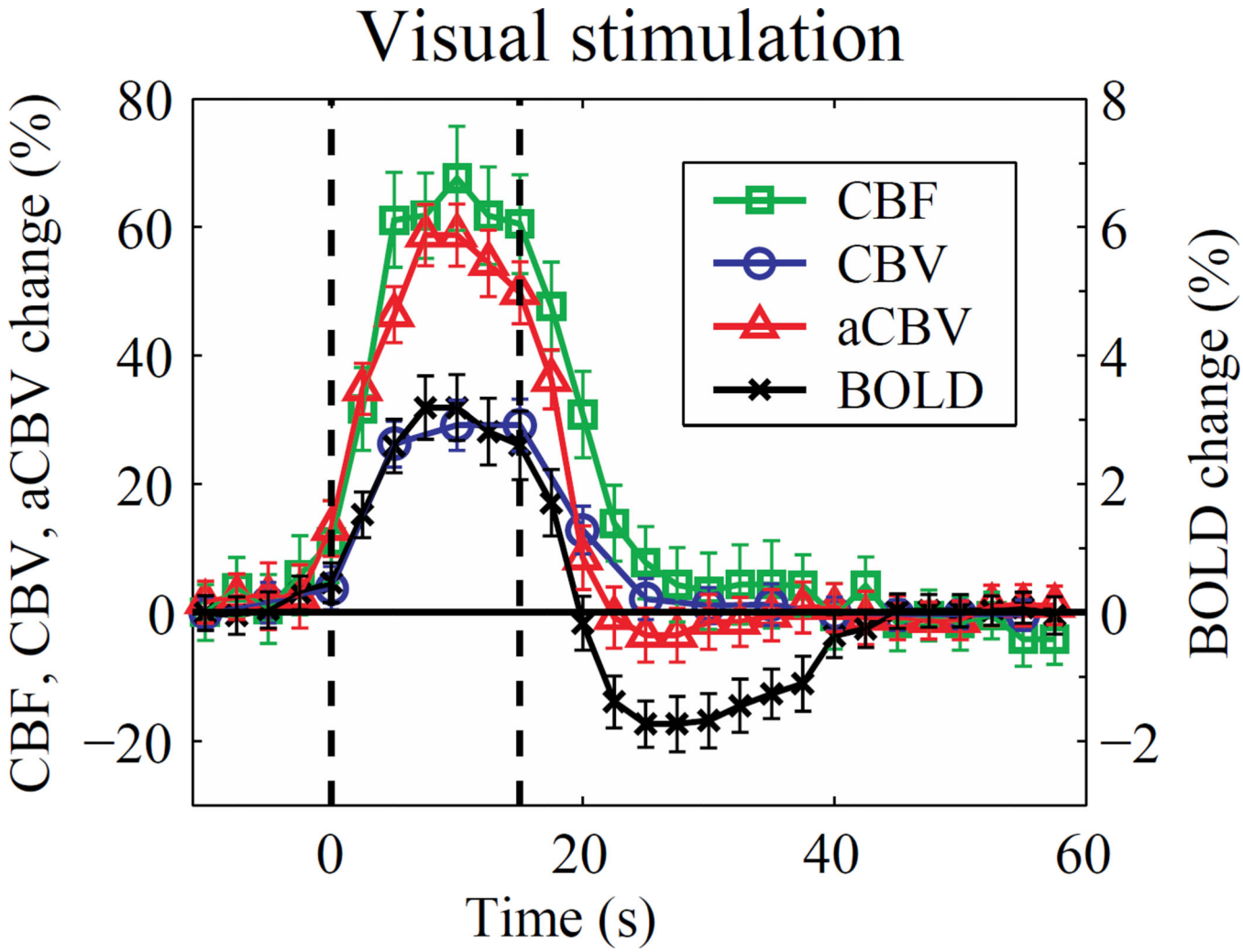

Figure 8. Evaluating the hemodynamic response to visual stimulation using 3.0T MRI

Mean time courses of cerebral blood flow (CBF, square), cerebral blood volume (CBV; circle), arterial CBV (aCBV; triangle), and blood oxygenation level-dependent (BOLD; cross) evolution during visual stimulation (flashing checkerboard) acquired at 3.0T from ASL, iVASO, and BOLD data. Time courses were first averaged over four repeated blocks of stimulation and subsequently over 10 healthy adults. Error bars represent inter-subject standard deviation. These data suggest that at intermediate field strength (e.g., 3.0T) and typical fMRI spatial resolutions (3 mm isotropic), the CBF and aCBV response increases slightly earlier than the BOLD and total CBV signal and also returns to baseline during the period of the BOLD post-stimulus undershoot. At higher spatial resolution and across cortical layers, these relationships may differ however. Data provided by Jun Hua; additional information on these relationships can be found in (Hua et al., 2011a; Hua et al., 2011c).

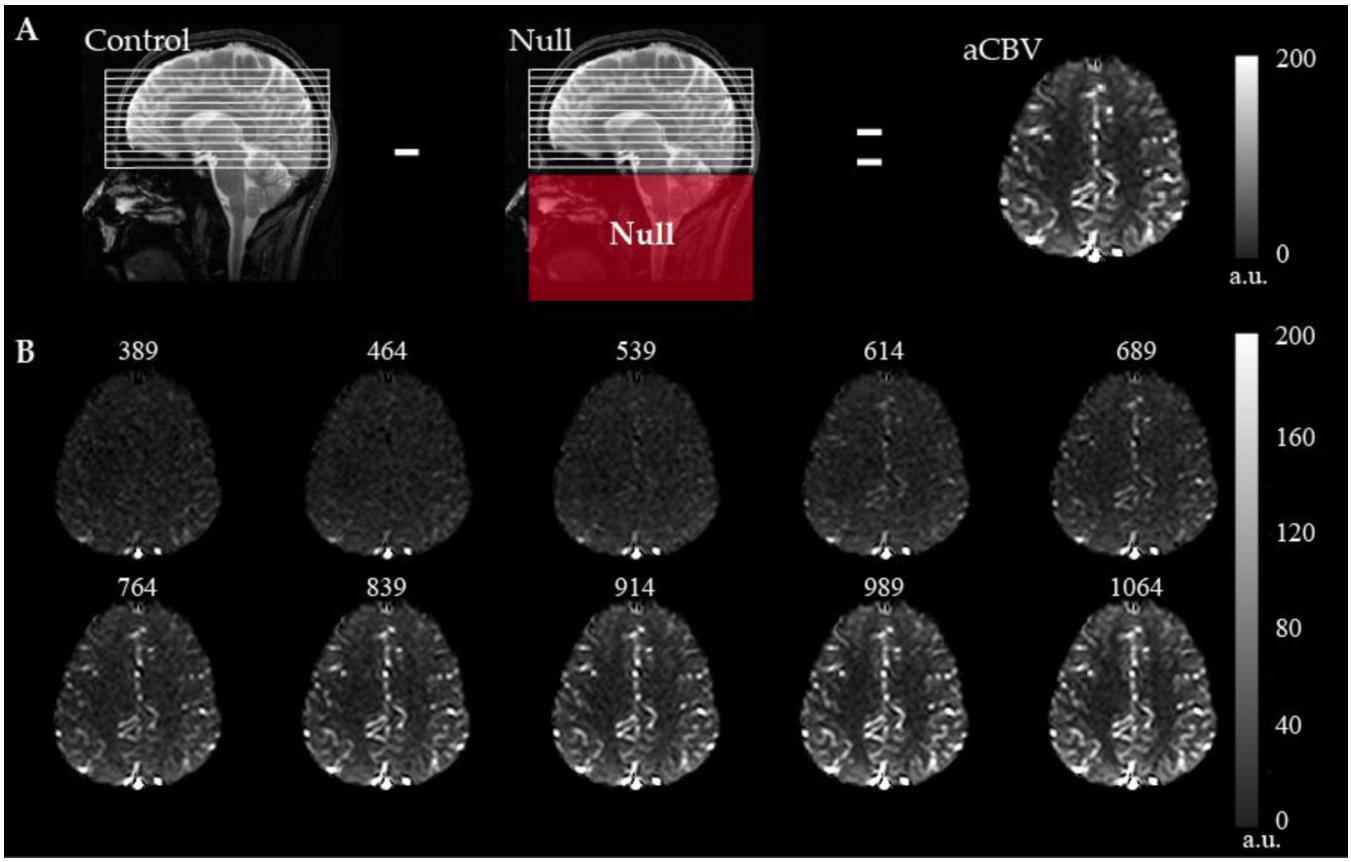

Figure 9. Inflow vascular space occupancy (iVASO) with dynamic subtraction (iVASO-DS)

A typical iVASO image is interleaved with an image when inflowing blood water is not inverted; if the image is acquired at the blood water null time [inversion time (TI) of approximately 300 – 1100 ms depending on repetition time (TR) choice], an absolute arterial CBV (aCBV) map can be obtained. (B) iVASO-DS images acquired for different TR/TI combinations, which show the inflow of blood water into the pre-capillary compartment. Additional information on absolute quantification of CBV from VASO subtraction procedures can be found in (Donahue et al., 2010b; Hua et al., 2011b).

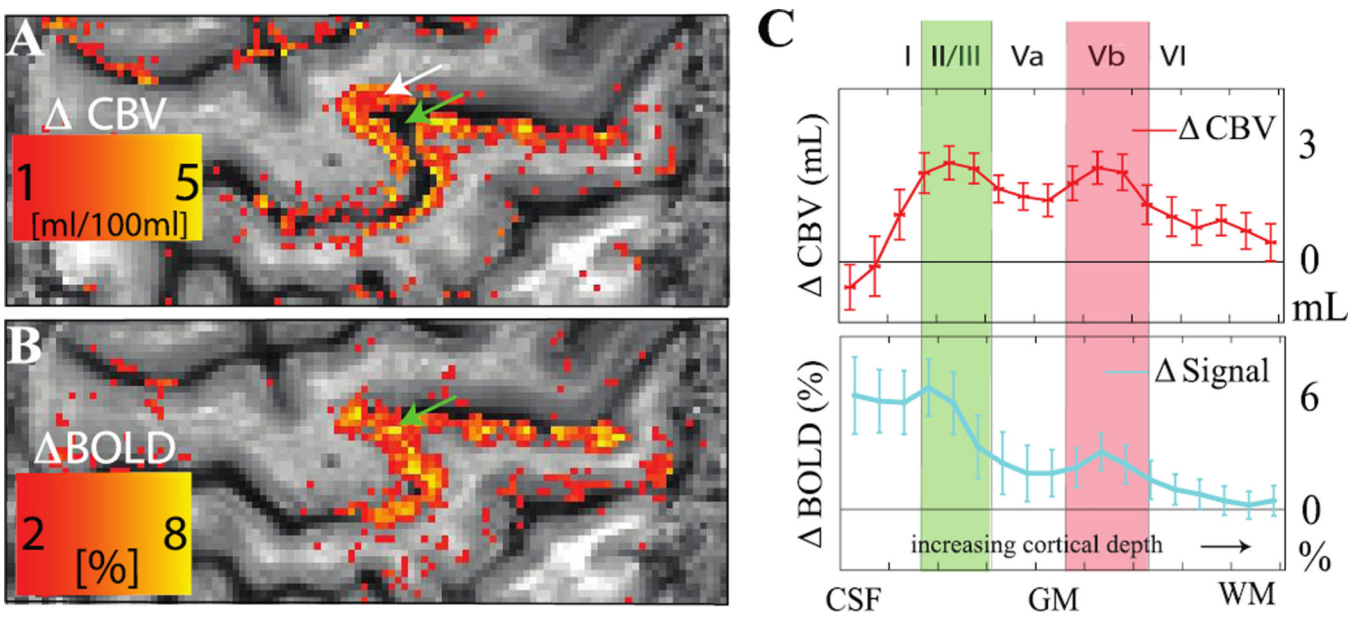

Figure 10. Improved spatial specificity of cerebral blood volume (CBV)-weighted vascular space occupancy (VASO) relative to blood oxygenation level-dependent (BOLD) fMRI

Human data acquired over motor and sensorimotor cortex (spatial resolution = 0.75 × 0.75 × 1.5 mm^3) at 7T during alternating periods of rest (30s) and finger tapping (30s). VASO data (A) reveal signal changes that are largely localized to gray matter (white arrow), whereas the BOLD data contain more diffuse and less specific contributions across the cortex and even within the sulcus (green arrow). Both the CBV-weighted VASO and BOLD responses as a function of cortical depth (C) show expected laminar differences in hemodynamic response, however the BOLD responses are less conspicuous, likely owing to additional contributions from draining veins and cerebrospinal fluid (CSF). The error bars refer to standard deviation of the response within the activated M1 area. Data provided by Laurentius Huber; additional information can be found in (Huber et al., 2016b).

Table 1

Summary of typical values used in quantification routines outlined in the text. References are intended to be representative and are not comprehensive owing to the extremely large range of studies quantifying these parameters.

Parameter	Value	Reference
MRI relaxation times (3.0T)		
T_1 of arterial blood water (Y = 0.92 ± 0.07; Hct = 0.42)	1664 ms	(Lu et al., 2004a)
T_2 arterial blood water (Y = 0.92 – 0.99; Hct=0.44)	96 – 122 ms	(Zhao et al., 2007)
T_2* of arterial blood water (Y = 0.92 – 0.99; Hct=0.44)	49–55 ms	(Zhao et al., 2007)
T_1 of venous blood water (Y = 0.69 ± 0.08; Hct=0.42)	1584 ms	(Lu et al., 2004a)
T_2 of venous blood (Y = 0.51 – 0.65; Hct=0.44)	23–35 ms	(Zhao et al., 2007)
T_2* of venous blood water (Y = 0.51 – 0.65; Hct=0.44)	15–22 ms	(Zhao et al., 2007)
T_1 of gray matter	1209 ms	(Lu et al., 2005)
T_2 of gray matter	71 ms	(Donahue et al., 2006)
T_1 of white matter	758 ms	(Lu et al., 2005)
T_2 of white matter	81 ms	(Lu et al., 2005)
T_1 of CSF	4300 ms	(Lu et al., 2005)
T_2 of CSF	1442–2000 ms	(Donahue et al., 2006; Gabr et al., 2016; Lu et al., 2005)
Physiological constants		
Blood brain partition coefficient: λ	0.9 ml blood / g tissue	(Herscovitch and Raichle, 1985)
Water density of gray matter: C_{GM}	0.89 ml water / ml tissue	(Lu et al., 2002)
Water density of blood: C_b	C_b=0.95–0.22•Hct ml water / ml blood	(Herscovitch and Raichle, 1985) (Lu et al., 2002)
Water density of CSF: C_{CSF}	1 ml water / ml CSF	(Donahue et al., 2006)
Healthy ranges of physiological parameters		
Bolus arrival time (BAT)	700–1500 ms	(Donahue et al., 2014b; MacIntosh et al., 2010; Mildner et al., 2014; Petersen et al., 2010; Wong et al., 1997)
Basal gray matter CBF	40–60 ml blood / 100g tissue / min	(Grubb et al., 1974; Petersen et al., 2010)
Basal white matter CBF	16–30 ml blood / 100g tissue / min	(Grubb et al., 1974; van Osch et al., 2009)
Basal gray matter CBV	0.047–0.055 ml blood / ml parenchyma	(Donahue et al., 2010b; Grubb et al., 1974; Grubb et al., 1978; Lu et al., 2003)
Basal white matter CBV	0.019 – 0.028 ml blood / ml parenchyma	(Grubb et al., 1974; Grubb et al., 1978)
Fractional gray matter CBF response to strong neuronal	5–100%	(Donahue et al., 2009a; Gonzalez-At et al., 2000)

Parameter	Value	Reference
stimulation		
Fractional total gray matter CBV response to strong neuronal stimulation	5–55%	(Ciris et al., 2014; Donahue et al., 2009a; Guidi et al., 2016; Hua et al., 2009; Hua et al., 2011a; Huber et al., 2016a)
Oxygen extraction fraction (OEF)	0.30 – 0.40	(Jordan et al., 2016; Lu et al., 2011; Powers et al., 1985)
Cerebral metabolic rate of oxygen consumption ($CMRO_2$)	2 – 4 ml oxygen / 100g tissue / min	(Lu et al., 2011; Maeda et al., 2015; Perlmutter et al., 1987; Powers et al., 1985)
Macrovascular hematocrit: Hct	38.5 – 50 % (male) 34.9 – 44.5 % (female)	(Adamson and Finch, 1975; Beck, 1991; Guyton, 1977)
Total hemoglobin: Hb	13.8 – 17.2 g/dL (male) 12.1 – 15.1 g/dL (female)	(Beck, 1991; Guyton, 1977)
Arterial blood oxygenation: Y_a	0.94 – 1.00	(Adamson and Finch, 1975; Beck, 1991; Guyton, 1977; Lu et al., 2011)
Venous blood oxygenation: Y_v	0.52 – 0.69	(Guyton, 1977; Lu et al., 2011)